Effective models of nonsingular quantum black holes

M. Cadoni,[*] M. Oi,[†] and A. P. Sanna[‡]

Dipartimento di Fisica, Università di Cagliari, Cittadella Universitaria, 09042 Monserrato, Italy and I.N.F.N, Sezione di Cagliari, Cittadella Universitaria, 09042 Monserrato, Italy

(Received 26 April 2022; accepted 6 July 2022; published 18 July 2022)

We investigate how the resolution of the singularity problem for the Schwarzschild black hole could be related to the presence of quantum gravity effects at horizon scales. Motivated by the analogy with the cosmological Schwarzschild-de Sitter solution, we construct a broad class of nonsingular, static, asymptotically flat black-hole solutions with a de Sitter (dS) core, sourced by an anisotropic fluid, which effectively encodes the quantum corrections. The latter are parametrized by a single length-scale ℓ, which has a dual interpretation as an effective "quantum hair" and as the length-scale resolving the classical singularity. Depending on the value of ℓ, these solutions can have two horizons, be extremal (when the two horizons merge) or be horizonless exotic stars. We also investigate the thermodynamic behavior of our black-hole solutions and propose a generalization of the area law in order to account for their entropy. We find a second-order phase transition near extremality, when ℓ is of order of the classical Schwarzschild radius R_S. Black holes with $\ell \sim R_S$ are thermodynamically preferred with respect to those with $\ell \ll R_S$, supporting the relevance of quantum corrections at horizon scales. We also find that the extremal configuration is a zero-temperature, zero-entropy state with its near-horizon geometry factorizing as $AdS_2 \times S^2$, signalizing the possible relevance of these models for the information paradox. Finally, we show that the presence of quantum corrections with $\ell \sim R_S$ have observable phenomenological signatures in the photon orbits and in the quasinormal modes (QNMs) spectrum. In particular, in the near-extremal regime, the imaginary part of the QNMs spectrum scales with the temperature as $c_1/\ell + c_2 \ell T_H^2$, while it goes to zero linearly in the near-horizon limit. Our general findings are confirmed by revisiting two already known models, which are particular cases of our general class of models, namely the Hayward and Gaussian-core black holes.

DOI: 10.1103/PhysRevD.106.024030

I. INTRODUCTION

Since the discovery of the Schwarzschild solution, the presence of a singularity inside black holes, together with the initial cosmological one, has represented a serious challenge to our current understanding of the fundamental laws of physics. This problem became even more serious after the groundbreaking Penrose and Hawking singularity theorems [1,2]. They proved incontrovertibly that, under a set of a few, very general and physically motivated assumptions (the validity of the weak energy condition and either global hyperbolicity or the validity of the strong energy condition), these space-time singularities are unavoidable, at least in the classical general relativity (GR) framework. Despite this, it is conjectured that these singularities are always hidden behind a causal barrier, the event horizon, which prevents outside observers from seeing them and the theory from completely loosing its predictive power [3]. Semiclassical effects, like black hole evaporation [4], seem however to bring the singularity problem back on the table, as the final steps of the evaporation process, where the singularity role should be most prominent, are still poorly understood.

Although it is in principle solvable already in the classical GR framework by relaxing some assumptions of Penrose's theorem and constructing nonsingular effective models (see, e.g., Refs. [5–11]; for models with nonlinearly coupled electromagnetic fields, see [12–17]) the singularity problem calls for the need of a quantum description of gravitational interactions. The most widely adopted approach in the past has been to assume that these quantum corrections should only be relevant at Planck scale, $\ell_P = \sqrt{G} \sim 10^{-35}$ m[1] [18–32]. Quantum gravity effects should become important only when the Compton length of a pointlike mass M becomes comparable with its Schwarzschild radius, $R_S = 2GM$. Thus, they should be irrelevant as long as gravitational interactions at

[*]mariano.cadoni@ca.infn.it
[†]mauro.oi@ca.infn.it
[‡]asanna@dsf.unica.it

[1]We adopt natural units, $c = \hbar = 1$. We will use G or ℓ_P^2 interchangeably.

Planck-scale distances are not considered, like the final stages of the evaporation of black holes, the behavior of space-time near their central singularity or the initial phases of the evolution of the universe.

In recent times, however, there have been many indications supporting the possibility of having relevant quantum gravity effects even at scales much larger than ℓ_P, i.e., at horizon or cosmological scales. At the black-hole level, this new perspective gains motivation from different approaches: the firewall paradox [33], which triggered several recent advances in tackling the black-hole information puzzle (islands and replica wormholes [34–37], nonlocal modifications of effective field theory [38–40], fuzzball proposal [41–43]); the emergent gravity and corpuscular gravity scenarios [44–50], in which a black hole is considered as a coherent state of a large number of gravitons of typical wavelength $\sim R_S$ [51–53]; finally, the quasinormal modes (QNMs) spectrum of the Schwarzschild black hole, whose description is consistent with that of an ensemble of oscillators with typical frequency $\omega \sim 1/R_S$ [54,55]. Further evidence came from the galactic and cosmological framework, where deviations from Newtonian dynamics and the evolution of dark energy can be interpreted in terms of long-range quantum gravity effects, described by an exotic source of Einstein's equation in the form of an anisotropic fluid [44,56–61].

The possibility of having quantum-gravity effects operating at black-hole horizon scales is also extremely interesting from a phenomenological point of view. These effects are expected to be encoded in the QNMs spectrum and to be detected by the next generation of gravitational wave (GW) detectors, like the Einstein Telescope (ET), in the ringdown phase of two compact objects merging to form a single black hole. In some particular cases, a manifest signature could be the presence of echoes in the GW signal [62–64].

The starting idea of this paper is that the resolution of the singularity problem could be related to the presence of quantum gravity effects at horizon scales. This is somehow natural because we expect quantum effects to be at work both in the smearing of the classical black-hole singularity and in generating an effective *quantum hair* at horizon scales. We parametrize the smearing of the classical singularity with a length-scale $\hat{L}$, whereas the quantum hair is represented by an extra length-scale ℓ. We assume that this smearing is sourced by an exotic form of matter having the form of an anisotropic fluid, which should give an effective description of quantum gravity effects. The analogy with galactic dynamics, where an infrared (IR) scale $R_0 = \sqrt{R_S L}$ is generated out of R_S and the size of the cosmological horizon L [44], now suggests that, similarly, ℓ can be interpreted as an IR scale generated from R_S and $\hat{L}$, for instance by the simple relation

$$\ell = R_S^a \hat{L}^b \tag{1}$$

with $a + b = 1$. Thus, the origin of the quantum hair ℓ should find explanation in the multiscale behavior of gravitational interactions.

Following the cosmological analogy, we can think of a nonsingular black hole as a "reversed" Schwarzschild-de Sitter (SdS) space-time, in which the external cosmological horizon and the inner Schwarzschild one are interchanged, and for which the length-scale $\hat{L}$ becomes the de Sitter (dS) length. In this way, we are motivated to construct a general class of nonsingular, static, asymptotically-flat black-hole solutions with a dS core, sourced by an anisotropic fluid, which endows the classical Schwarzschild solution with a quantum hair ℓ. Extending this similarity with the SdS case and with the dynamically generated scale R_0, we will explicitly prove that ℓ is dynamically generated by R_S and $\hat{L}$ by $\ell \sim R_S^{1/3} \hat{L}^{2/3}$, a relation which should hold in general for regular models with dS cores.

We find that imposing a regular dS core (a) always violates the strong energy condition in the interior of these objects, and therefore allows us to circumvent the singularity theorem, and (b) depending on the value of the parameter ℓ, our nonsingular models can have two, one (extremal configuration) or no horizons. We then proceed by investigating the implications of the presence an extra parameter ℓ, assumed to be of the same order of magnitude as R_S, on the thermodynamic properties of the black hole and on the phenomenology of the models, i.e., on photon orbits and on the QNMs spectrum.

By using the first law of thermodynamics, we show that the presence of ℓ causes deviations from the standard area law. We propose therefore an entropy formula to generalize the latter. Using this general entropy formula, we also find that the extremal configuration is a zero-temperature, zero-entropy state, a behavior drastically different from extremal Reissner-Nordström (RN) and Kerr black holes. This, together with the fact that the extremal, near-horizon, geometry factorizes as the tensor product of two-dimensional Anti de Sitter (AdS_2) with a two-sphere, i.e., $AdS_2 \times S^2$, indicates that these regular models could actually be relevant for tackling the information paradox [35,65–69]. By investigating the behavior of the specific heat and the free energy of the hole, we find a second-order phase transition near extremality, i.e., for $\ell \sim R_S$. In particular, black holes with $\ell \sim R_S$ are energetically preferred with respect to those with $R_S \gg \ell$, lending further support to the possible relevance of quantum corrections at horizon scale.

On the phenomenological side, we find that, for black holes with $\ell \ll R_S$, deviations from standard results concerning photon orbits and the QNMs spectrum are negligibly small and not detectable, at least in the near future. Conversely, black holes with $\ell \sim R_S$ are characterized by macroscopic deviations from the Schwarzschild behavior, whose signatures are potentially detectable by the next generation of GW detectors. In particular, by analytically computing the QNMs spectrum in the eikonal

approximation, we find that, in the near-extremal limit, the imaginary part of the quasinormal frequencies scale with the black-hole temperature as $c_1/\ell + c_2 \ell T_H^2$ (with $c_{1,2}$ constants), while in the near-extremal and near-horizon regimes, it goes to zero, in agreement with several results in the literature [70–81]. This appears to be a general feature of nonsingular black holes, common also to charged and/or rotating extension of regular models [82–84].

In the final part of the paper, we check our results by revisiting two already-known models, namely the Hayward and Gaussian-core black-hole metrics, which represent particular cases of our general class of regular black holes.

The outline of the paper is the following. In Sec. II we build up the grounds for our multiscale description of gravity by drawing an analogy between the SdS solution and galactic dynamics from one side, and regular black-hole models for the other side.

In Sec. III, we find the exact, most-general, spherically-symmetric static solution of Einstein's field equations, sourced by an anisotropic fluid, and we outline the basic requirements needed to avoid the central singularity. We then focus on a subclass of such models by choosing a particular equation of state and analyze the null and strong energy conditions.

In Sec. IV, we select the general class of regular black-hole solutions by imposing a set of minimal constraints, namely dS behavior in the interior, asymptotically flatness at infinity and the presence of horizons. We also study the general thermodynamic behavior of these models, discussing the first law of thermodynamics and the appearance of the second-order phase transition. Finally, we investigate photon orbits and the QNMs spectrum in the eikonal approximation.

In Sec. V and Sec. VI the general discussion is applied and the results are confirmed by revisiting two previously-proposed regular black-hole models, the Hayward and the Gaussian-core ones, which appear as particular cases of our general class of models. We finally state our conclusions in Sec. VII.

II. UNIFIED DESCRIPTION OF SPACE-TIME AND MATTER INSIDE A BLACK HOLE

As anticipated in the Introduction, in the present paper we adopt a description of gravitational interactions in terms of an effective multiscale field theory, characterized by the generations of hierarchically different length-scales.

This description is natural in the cosmological and galactic context, as gravity and baryonic matter are characterized by: (1) the Planck length ℓ_P, (2) the size of the cosmological horizon L, related to the cosmological constant by $L = \Lambda^{-1/2}$, and (3) the gravitational radius of a clump of baryonic matter with mass M, $R_S \sim \ell_P^2 M$. As already mentioned, an intermediate (mesoscopic) IR length scale in the galactic regime

$$R_0 = \sqrt{R_S L} \tag{2}$$

is dynamically generated from R_S and L. At this scale, gravity deviates from its Newtonian behavior as it is evident from rotational curves of galaxies. Moreover,R_0 can be seen as a scale at which long-range quantum gravity effects become relevant [44,56–58]. This scenario allows for an effective description in the GR framework in terms of an anisotropic fluid, which can be seen as a two-fluid model of dark energy and matter [56–61]. The resulting space-time is the SdS solution, in which dark energy dominates at very large scale. In this regime, we have a description in terms of the pure dS space-time and a related scale isometry [85]. When instead clustered matter M is present and becomes non-negligible, the scale invariance of the dS-background is broken, the quantum scale R_0 is generated and we have an effective description in terms of the SdS space-time. The latter is characterized by an internal Schwarzschild-like horizon, determined by the baryonic mass M, and by an external dS horizon, which, for small M, is located at $r = L$. The short-scale regime, instead, is described by the Schwarzschild solution with a related scale R_S, at which the matter contribution dominates over dark energy. The geometry is asymptotically dS.[2]

In the emergent gravity scenario of Ref. [44], these two regimes are assumed to be endowed with a microscopic description in terms of quantum gravity degrees of freedom (DOFs) entangled on short-scales (at $r \sim R_S$) and on cosmological scales ($r \sim L$). Following Refs. [44,56], the short-range entanglement is responsible for the holographic horizon-area scaling of the entropy. The long-range regime is, instead, characterized by the slow thermalization of IR, long-range interacting, quantum-gravity DOFs. This IR dynamics is responsible for an extensive, i.e., *volume*-dependent, contribution to the entropy. As argued in Ref. [44], the competition between the area- and volume-laws in the entropy generates a mesoscopic scale R_0 and an additional gravitational dark force explaining the deviations from the Newtonian dynamics at galactic scales. This multiscale description of gravity, with a "fast scale," R_S and a "slow scale" L, is reminiscent of thermodynamic systems characterized by a glass transition [44].[3]

Following this line of reasoning, one is led by analogy to use a similar multiscale description of matter and gravity for the black-hole interior, in particular to solve the singularity problem. We will consider only macroscopic black holes, i.e., black holes whose horizon radius is hierarchically larger than ℓ_P. The short-distance behavior

[2]Notice that, in order to make contact with a black hole space-time, we have to use a static parametrization of the dS geometry.

[3]At short time scales, glassy systems have properties which cannot be distinguished from those of crystals: their effective descriptions are identical. However, the former are characterized by a long timescale behavior, which makes them completely different from crystals.

in the black-hole interior (near the singularity) is now dominated by the short-scale dynamics of the emergent space-time DOFs. It is natural to assume that, similarly to the cosmological case at large scales, here the contribution of matter is negligible at short scales, where we have an effective GR description in terms of a pure dS space-time. This regime is therefore characterized by an ultraviolet (UV) dS length $\hat{L}$, a related cosmological constant $\hat{\Lambda} = \hat{L}^{-2}$ and scale invariance. This description is fully consistent with the existence of an UV fixed point, predicted by the quantum-gravity asymptotic safety scenario (see, e.g., Refs. [86–88]; for a resolution of the classical singularity in the asymptotic safety scenario, see Ref. [89]; for recent results on scale invariance in the core of black holes, see Ref. [90]). Moreover, the dS behavior of the space-time at short scales is consistent with volume-law contribution to the entropy.

Introducing baryonic matter M breaks the scale and conformal invariance of the dS space-time in the black-hole interior. Similarly to the galactic and cosmological regimes [58], in this case a new quantum scale ℓ is generated in terms of $\hat{L}$ and R_S. Using an argument similar to that of Ref. [44], the generation of ℓ can be also explained in terms of the competition between the short-range, volume contribution and the area-law-Bekenstein-Hawking contribution to the entropy we have at large distances from the center, at the Schwarzschild radius R_S.

We see therefore that a multiscale description of gravitational interactions can be adopted both to describe black-holes in a cosmological background and the interior of asymptotically flat black holes. In the two cases, however, the horizon positions are reversed. In the latter case, the dS horizon is the internal one, whereas the matter-determined horizon is the external one. For this reason, even if we expect $\ell = f(\hat{L}, R_S)$, this relation needs not to be the same as that relating R_0, L, and R_S in Eq. (2). Another difference from the cosmological SdS case, is that here we have the possibility of an external description, i.e., a description of an asymptotic observer at $r \to \infty$. The latter sees "quantum" deviations from the Schwarzschild geometry, parametrized by ℓ. In this respect, it should be emphasized once again that the relation between the cosmological case, described by Eq. (2), and the black-hole case, described instead by Eq. (1), is that of an analogy. In particular, this prevents one from finding any relation between the cosmological scales (L, R_0) and our scales $(\hat{L}, \ell)$.

From this perspective, we have a new phase in the black-hole interior, in which the emergent gravity DOFs and matter should allow for an effective two-fluids description, i.e., an effective description in terms of an anisotropic fluid [91]. In the next sections, we will construct a general class of GR models describing gravity sourced by an anisotropic fluid, which allows for nonsingular black-hole solutions with two event horizons and an internal dS core.

III. SPHERICALLY SYMMETRIC SOLUTIONS SOURCED BY ANISOTROPIC FLUIDS

Our starting point is GR sourced by an anisotropic fluid. The stress-energy tensor $T_{\mu\nu}$ appearing in Einstein's equations $G_{\mu\nu} = 8\pi G T_{\mu\nu}$ will be that pertaining to an anisotropic fluid. Anisotropic fluids have a long history and have been fruitfully used in several different contexts in gravitational studies, including compact objects, singular and nonsingular black hole models, cosmology (for an incomplete list, see, e.g., Refs. [8,11,22,57,59–61,91–104]).

We consider static, spherically-symmetric solutions of the theory, whose metric part can be written in the form

$$ds^2 = -e^{\nu(r)}dt^2 + e^{\lambda(r)}dr^2 + r^2 d\Omega^2;$$
$$d\Omega^2 = d\theta^2 + \sin^2\theta d\phi^2. \tag{3}$$

where $\nu(r)$ and $\lambda(r)$ are metric functions, depending on the radial coordinate r only.

The stress-energy tensor describing the anisotropic fluid can be written as [92]

$$T_{\mu\nu} = (\epsilon + p_\perp)u_\mu u_\nu + p_\perp g_{\mu\nu} - (p_\perp - p_\parallel)w_\mu w_\nu, \tag{4}$$

where $\epsilon(r)$, $p_\parallel(r)$, and $p_\perp(r)$ are the energy density and the radial and tangential pressure components, respectively, while u_μ and w_μ are 4-vectors satisfying the normalization conditions $g^{\mu\nu}u_\mu u_\nu = -1$, $g^{\mu\nu}w_\mu w_\nu = 1$, and $u^\mu w_\mu = 0$.

The independent Einstein's field and stress-energy tensor conservation equations read (the prime denotes derivation with respect to r)

$$\frac{1 - e^{-\lambda} + re^{-\lambda}\lambda'}{r^2} = 8\pi G\epsilon; \tag{5a}$$

$$\frac{e^{-\lambda} - 1 + re^{-\lambda}\nu'}{r^2} = 8\pi G p_\parallel; \tag{5b}$$

$$p_\parallel' + \frac{\nu'}{2}(\epsilon + p_\parallel) + \frac{2}{r}(p_\parallel - p_\perp) = 0. \tag{5c}$$

Integration of the first equation yields

$$e^{-\lambda(r)} = 1 - \frac{8\pi G}{r}\int \epsilon r^2 dr \equiv 1 - \frac{2Gm(r)}{r} \tag{6}$$

where $m(r)$ is the Misner-Sharp (MS) mass

$$m(r) \equiv 4\pi \int_0^r d\tilde{r}\tilde{r}^2\epsilon(\tilde{r}). \tag{7}$$

Using Eq. (7), Eq. (5b) can be recast in the more useful form

$$\frac{\nu'}{2} = \frac{4\pi G p_{\parallel} r^3 + Gm}{r(r-2Gm)}. \tag{8}$$

The system (5a)–(5c) is not closed. In order to determine the solution unambiguously, we must support Eqs. (5a) and (5c) with two further equations. The simplest and physically natural way to close the dynamical system is to provide: (1) a barotropic equation of state (EoS) for the radial pressure $p_{\parallel} = p_{\parallel}(\epsilon)$ and (2) the matter density profile $\epsilon(r)$. In the following, we will fix the equation of state and the matter density profile by imposing absence of singularities, Schwarzschild behavior at $r \to \infty$ and using the analogy with cosmology discussed in Sec. II.

A. Equation of state and energy conditions

The simplest and most natural EoS we can choose is

$$p_{\parallel} = -\epsilon. \tag{9}$$

This choice is physically well motivated by the analogy with the cosmological and galactic regime, since it allows both for a dS and SdS (cosmological) phases. It allows for a pure dS behavior near $r = 0$, which implies the absence of a singularity in the black-hole interior. Moreover, the EoS also allows for asymptotically-flat solutions at $r \to \infty$, when both $p_{\parallel} \to 0$ and $\epsilon \to 0$. One can now easily check that, using Eq. (5a) and Eq. (5b), the EoS (9) implies $\lambda(r) = -\nu(r)$. In the remainder of the paper, we will adopt the following parametrization of the metric functions $e^{\nu} = e^{-\lambda} = A(r)$.

Equation (8) can be readily integrated, using Eqs. (7) and (9), and yields

$$A(r) = 1 - \frac{2Gm(r)}{r}. \tag{10}$$

Finally, using Eqs. (5c), (7) and (9), we can express the fluid anisotropy $p_{\perp} - p_{\parallel}$ as a function of the MS mass as follows

$$\frac{p_{\perp} - p_{\parallel}}{r} = \frac{1}{4\pi r^3}\left(m' - \frac{rm''}{2}\right). \tag{11}$$

It is useful to write down explicitly the energy conditions for the specific case in which the EoS (9) holds.

1. Null energy condition (NEC)

In order this condition to be satisfied, we have to require that both $\epsilon + p_{\parallel} \geq 0$, $\epsilon + p_{\perp} \geq 0$ hold globally [105]. The first is trivially satisfied due to Eq. (9), while the second one reduces to

$$\epsilon'(r) \leq 0, \tag{12}$$

upon using Eqs. (7) and (11).

2. Strong energy condition (SEC)

In this case, we have to require $\epsilon + p_{\parallel} + 2p_{\perp} \geq 0$ to hold globally [105]. Together with Eqs. (7) and (11), this requirement reduces to

$$2r\epsilon(r) + r^2\epsilon'(r) \leq 0. \tag{13}$$

B. Absence of singularity and behavior near $r = 0$

In order to avoid the presence of a central singularity at $r = 0$ we first impose a set of minimal, very general requirements on the form of the metric functions and on the density and pressure profiles:

(i) Regularity of $e^{-\lambda}$ in $r = 0$ together with Eqs. (6) and (10) require $m(r) \to 0$ sufficiently fast for $r \to 0$;
(ii) Regularity of $p_{\parallel}$ in $r = 0$ together with Eq. (8) require $r\nu' \to 0$ sufficiently fast for $r \to 0$;
(iii) We also require both $p_{\parallel}$ and $p'_{\parallel}$ to be smooth in $r = 0$. From Eq. (5c), this implies the regularity condition for the tangential pressure component

$$\lim_{r\to 0} \frac{p_{\perp} - p_{\parallel}}{r} = 0. \tag{14}$$

Equation (14), together with Eq. (11), implies the following behavior near $r = 0$ for the mass function $m(r)$

$$m(r) \sim m_1 + \frac{r^3}{2\ell_{\mathrm{P}}^2 \hat{L}^2} + \mathcal{O}(r^4) \quad \text{for } r \to 0 \tag{15}$$

with m_1 and $\hat{L}$ some integration constants. Absence of curvature singularity for the metric in $r = 0$ requires $m_1 = 0$. The other term, proportional to r^3, instead, gives a local dS solution with a dS length $\hat{L}$

$$A(r) \sim 1 - \frac{r^2}{\hat{L}^2} + \mathcal{O}(r^3) \quad \text{for } r \to 0. \tag{16}$$

This dS description of the solution core is fully consistent with both the EoS (9) and the analogy with the SdS solution in cosmology (see, e.g., Ref. [8] for a regular model with a Minkowski core).

C. Asymptotic flatness and behavior at $r \to \infty$

In the asymptotic ($r \to \infty$) region, our solution must be indistinguishable from the Schwarzschild solution. This implies the space-time to be asymptotically flat, with a subleading Schwarzschild term in the metric function $A(r)$. Moreover, the two pressure components $p_{\parallel}$ and $p_{\perp}$ have to vanish in the limit $r \to \infty$. Equation (11) implies that the minimal condition to have $p_{\perp} \to 0$ is

$$m = \mathcal{C}_0 r^2 + \mathcal{C}_2 r + M + \mathcal{O}\left(\frac{1}{r}\right), \tag{17}$$

with $\mathcal{C}_0$, $\mathcal{C}_2$ and M integration constants. Asymptotic flatness and absence of conical defects require $\mathcal{C}_0 = \mathcal{C}_2 = 0$, whereas M becomes the Arnowitt-Deser-Misner (ADM) mass of the solution measured by the asymptotic observer,

$$m = M + \mathcal{O}\left(\frac{1}{r}\right) \quad \text{for } r \to \infty. \tag{18}$$

We will also assume that the function $m(r)$ interpolates smoothly between the near $r = 0$ dS behavior and flat space-time at $r \to \infty$.

IV. A GENERAL CLASS OF NONSINGULAR QUANTUM BLACK-HOLE MODELS

Absence of a central singularity and the requirement of a Schwarzschild asymptotic behavior strongly constrain, through Eqs. (16) and (18), the local form of the mass function $m(r)$ [or, equivalently, of the metric function $A(r)$] near $r = 0$ and $r \to \infty$. However, the global behavior of $m(r)$, which interpolates between $r = 0$ and $r \to \infty$, remains extremely weakly constrained. In this section, we will use the analogy with the cosmological, SdS case to further constrain its global form. We will get, as output, a general class of models, which can be used to give an effective description of quantum black holes.

Using the analogy with the cosmological case, we assume that $m(r)$ depends only on the two parameters $\hat{L}$ and R_S, which characterize its local behavior near $r = 0$ and near $r \to \infty$. This implies that the quantum IR scale ℓ can be written as a function of $\hat{L}$ and R_S only, $\ell = \ell(\hat{L}, R_S)$. The explicit relation between these three scales can be found using a simple argument. As our models interpolate between the scale-invariant dS behavior in the core and that of clustered matter, which gives the Schwarzschild solution at large radii, there will be a scale ℓ at which these two effects balance out. By exploiting the same arguments used in Ref. [58], we expect this scale to correspond to the one at which the Compton length associated to a test particle, with mass m, in the dS potential $V_{dS} = r^2/\hat{L}^2$, is of the same order of the Compton length of the same test particle in the Schwarzschild potential generated by the surrounding mass, i.e., $V_{Sch} = R_S/r$. The former, curing the singularity at the center, reads $\lambda_{c,dS} \sim \hbar/(|V_{dS}|m) = \hbar\hat{L}^2/r^2 m$, while the latter, instead, responsible for quantum correction at the horizon scale, is $\lambda_{c,Sch} = \hbar r/R_S m$. We thus have

$$\frac{\lambda_{c,dS}}{\lambda_{c,Sch}} \sim \mathcal{O}(1) \Rightarrow r \sim \ell \sim R_S^{1/3}\hat{L}^{2/3}, \tag{19}$$

which is a scaling relation of the form given in Eq. (1), with $a = 1/3$, $b = 2/3$. We will check this general results in two specific models in Sec. V and Sec. VI.

The presence of a new IR quantum scale implies that we have two complementary descriptions of the quantum black hole. A black-hole-interior description, based on the parameters $\hat{L}$ and M, and a black-hole-exterior one, based instead on ℓ and M. The second case corresponds to the classical description characterized by the classical hair M and by a quantum deformation parameter, i.e., the quantum hair ℓ.

A second requirement on the form of the function $m(r)$ comes from the analogy with the cosmological SdS space-time case. The space-time must allow for two horizons, an internal one at $r = r_-$—a dS-like horizon—and an external one at $r = r_+$—a Schwarzschild-like horizon. Depending on the value of the parameter ℓ (or, equivalently, of the parameter $\hat{L}$), we will have three cases: (1) a black hole with two horizons, (2) the two horizons merge and the black hole becomes extremal, and (3) a horizonless compact object.

We can easily estimate the relation between the parameters in the extremal case (2) using a very simple argument. For the internal observer, which describes its space-time as dS, the energy density is constant and given by $\epsilon \sim \frac{1}{\hat{L}^2\ell_P^2}$. The total energy inside a sphere of radius r is $E(r) \sim \frac{r^3}{\hat{L}^2\ell_P^2}$. For the extremal black hole, we must have $r \sim \hat{L}$ and the total energy inside the sphere must match the black-hole mass M seen by the outside observer: $E(L) \sim \frac{\hat{L}^3}{\hat{L}^2\ell_P^2} = M$. This equation, together with Eq. (19), implies that the extremal black hole must be characterized by

$$\ell \sim R_S \sim \hat{L}. \tag{20}$$

We find therefore that ℓ has both a quantum origin and should be of the same order of magnitude the Schwarzschild scale R_S.

For $\ell \lesssim R_S$, the presence of the dS core and asymptotic flatness force the metric to have an even number of horizons. In the following, we will limit ourselves to the case of only two horizons (see below). In the limit $\ell \to 0$, corresponding to $\hat{L} \to 0$, the inner dS horizon is pushed toward $r = 0$ and disappears: a singularity is generated in the center. The outer horizon, on the other hand, becomes the classical Schwarzschild one. This case corresponds to the classical limit of our model, in which the usual asymptotically flat Schwarzschild solution is recovered. In this regime, quantum effects can be neglected. In view of Eq. (18), the simplest way to recover the Schwarzschild solution in the $\ell \to 0$ limit is to assume that

$$m(r) = m\left(\frac{r}{\ell}, M\right). \tag{21}$$

Conversely, in the $\ell \to \infty$ limit, corresponding also to $\hat{L} \to \infty$, the outer horizon disappears and the space-time becomes dS. Notice that also $M \to \infty$ in this case,

consistently with the fact that we have a constant energy density. This is the cosmological regime of emergent gravity, in which dark energy in the form of the cosmological constant L^{-2} fully dominates [44]. Our description in terms of a quantum black hole with a dS interior sourced by an anisotropic fluid breaks down in this limit. An effective description of gravitational interactions in terms of GR sourced by an anisotropic fluid is still valid. It can be used to describe galactic dynamics and the generation of the IR length of galactic size (2), giving rise to interesting effects, like the emergence of a dark force at galactic level [56–58]. Finally, for $\ell \gtrsim R_S$, we have a solution with no horizons, which can be thought of as an horizonless star.

Let us now write down the most general form of the metric function satisfying the conditions discussed above and in Secs. III B and III C. We can parametrize the metric function $A(r)$ in terms of a smooth function F as follows:

$$A(r) = 1 - \frac{R_S}{\ell} F\left(\frac{r}{\ell}\right) \equiv 1 - \alpha F(y) \tag{22}$$

where we have defined the dimensionless coupling $\alpha \equiv R_S/\ell$ and radial coordinate $y \equiv r/\ell$. Furthermore, the function F must satisfy the following conditions:

(1) $$F(y) \sim \frac{1}{y} \quad \text{for } y \to \infty; \tag{23}$$

(2) $$F(y) \sim y^2 \quad \text{for } y \to 0; \tag{24}$$

(3) The equation $1 - \alpha F(y) = 0$ admits at most two real positive roots y_+, y_-. Moreover, parameter regions discriminated by α are present in which the equation allows for two distinct, a single one or no real positive roots.

When we have two roots y_+ corresponds to an event horizon while the inner horizon, given by y_-, is generally a Cauchy horizon. The presence of Cauchy horizons raised several concerns in the literature regarding the stability and the viability of such regular black-hole solutions with two horizons. Indeed, according to Poisson, Israel and Ori [106,107], the Cauchy horizon is typically exponentially unstable under perturbations, an effect known as "mass inflation." In standard regular-black-holes approaches with $\ell \sim \ell_P$, this instability develops in a time of order of the Planck time, which is a much shorter timescale than the evaporation time, challenging therefore the ability of these models to give a complete description of the whole evaporation process [108–110]. However, it has been shown recently [111] that a detailed analysis is needed in the nonsingular black-hole case and that the mass instability does not occur in some specific regular models, like those of Refs. [86,94][4] (but see also Ref. [115] for very recent results).

Apart from the three conditions above on the form of the function $F(y)$, we also introduce a constraint on the form of its derivative

(4) In the region $y \geq y_+$, $F'(y)/F$ has only one local extrema (a maximum).

The latter represents a statement on the behavior of the black hole temperature and is needed to have the simplest thermodynamic phase portrait (see Sec. IV C).

Finally, requiring the regular quantum-corrected metric to be an exact solution of some effective field equations derived from an action principle could place further constraints on the function F. These constraints are analyzed in Ref. [116]. The analysis is mainly concerned with possible quantum corrections to the Schwarzschild metric, assumed to be polynomial in $1/r$ at asymptotic infinity (even if the main results of the paper seem to hold even if the latter assumption is relaxed). These corrections are derived as asymptotic solutions of effective field equations derived from an Einstein-Hilbert action corrected by additional higher-order terms in the curvature. What is found is that, unless either fine-tuning is assumed or strong infrared nonlocalities in the gravitational action are taken into account, algebraic forms of F, like those of Refs. [8,94], for instance, are incompatible with a principle of least action. Therefore, their feasibility as "quantum-deformed" black holes may be questionable, at least if one requires these solutions to be derived from an Einstein-Hilbert action with higher-order terms in the curvature.

Condition 3 implies the existence of critical values α_c and y_c for α and y respectively, labeling the extremal case, when the two black-hole horizons merge. These critical values are determined by requiring the metric function to have a double-degenerate zero, i.e., by the system of equations,

$$1 - \alpha F(y) = 0, \qquad F'(y) = 0. \tag{25}$$

Notice that a simple principle of naturalness implies α_c and y_c being of order 1, so that the critical values for ℓ and r are of order R_S. Therefore, α_c allows us to distinguish three regimes for our model:

(a) $\alpha \gg \alpha_c$, corresponding to $\ell \ll R_S$ (i.e., $\ell \sim \ell_P$), which describes the Schwarzschild black hole with small quantum corrections [21–32];

(b) $\alpha \sim \alpha_c$, corresponding to $\ell \sim R_S$. In this case, ℓ parametrizes quantum gravity effects at horizon scales [41–50,54,55,74];

[4]We point the reader to Refs. [112–114] for an alternative regular model without the presence of an inner Cauchy horizons in the corpuscular gravity framework.

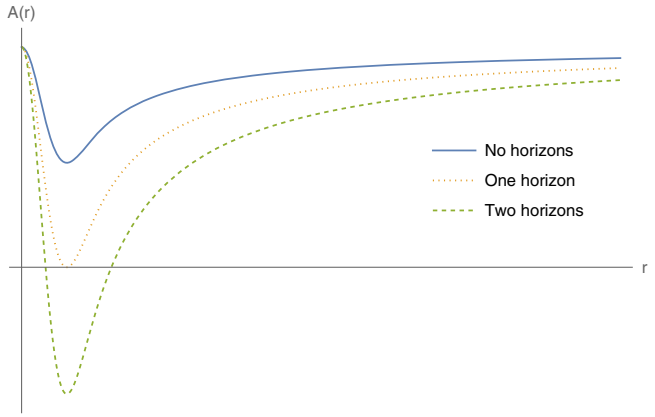

FIG. 1. Qualitative behavior of the metric function $A(r)$ as a function of the radial coordinate and for different values of the parameter α. We can either have solutions with no horizons for $\alpha < \alpha_c$ (blue solid curve), extremal solutions with a single horizon for $\alpha = \alpha_c$ (orange dotted curve) or solutions with two horizons for $\alpha > \alpha_c$ (green dashed curve).

(c) $\alpha < \alpha_c$, corresponding to $\ell > R_S$, which describes horizonless stars. We will not consider this case in the following.

A qualitative behavior of the metric function $A(r)$ in the three cases is plotted in Fig. 1.

A. Energy conditions

Given the form (22) for the general metric function and taking into account (23) and (24), we can rewrite the two energy conditions (12) and (13) in terms of the function F and discuss their behavior near $r \sim 0$ and for $r \to \infty$. Using Eqs. (6) and (22) in (12) and (13), we get

$$\epsilon' = -\frac{\alpha F}{4\pi G \ell^3 y^3} + \frac{\alpha F''}{8\pi G \ell^3 y} \leq 0; \tag{26a}$$

$$2r\epsilon + r^2\epsilon' = \frac{\alpha(2F' + yF'')}{8\pi G \ell} \leq 0. \tag{26b}$$

Near $y \sim 0$, $\epsilon' = 0$ follows, so that the NEC is satisfied, while $2r\epsilon + r^2\epsilon' \sim 0^+$ for $y \to 0$: the SEC is violated somewhere deep in the core of the astrophysical object. This is expected, since this violation is a characteristic of the dS spacetime.

On the other hand, for $y \to \infty$, using Eq. (23) we get $\epsilon' \sim 0$ and $2r\epsilon + r^2\epsilon' \sim 0$. Thus, the NEC and the SEC are satisfied in the asymptotic region, as expected in view of the Schwarzschild asymptotics of the solutions.

Violation of the SEC in the inner core explains how in our models the usual singularity theorems can be circumvented. Even if the dS behavior near $r = 0$ assures the absence of a curvature singularity at $r = 0$, in principle it is not sufficient to guarantee the geodesic completeness of the space-time described by the metric function (22). In the Appendix, we explicitly show that in our models, caustics of timelike geodesics cannot form, proving therefore the geodesic completeness of space-times described by Eq. (22).

B. Extremal limit

As it is usually the case for standard charged and/or rotating black holes [117–120], in the extremal limit and in the near-horizon approximation, the local geometry of our space-time behaves as $AdS_2 \times S^2$, i.e., as the tensor product of a two-dimensional (2D) AdS space-time and a two-sphere, with both the AdS_2 length L_2 and the radius of S^2 of order R_S. In fact, in the extremal limit $r_+ = r_- = r_c$, the metric function $A(r)$ must have a double zero at $r = r_c$, determined by the solution of Eq. (25). Expanding it near the horizon, i.e., in power series of $r - r_c$, we get at leading order

$$ds^2 = -L_2^{-2}(r-r_c)^2 dt^2 + L_2^2 (r-r_c)^{-2} dr^2 + r_c^2 d\Omega^2, \tag{27}$$

where we have defined $L_2^{-2} = -\frac{1}{2}A''(r_c)$ and $r_c \sim R_S$ owing to Eq. (20). Moreover, for purely dimensional reasons, the same equation implies $A(r_c)'' \sim R_S^{-2}$, from which $L_2 \sim R_S$ follows. A translation of the radial coordinate $r \to r + r_c$ brings the metric into the form

$$ds^2 = -\frac{r^2}{L_2^2} dt^2 + \frac{L_2^2}{r^2} dr^2 + r_c^2 d\Omega^2, \tag{28}$$

which describes an $AdS_2 \times S^2$ space-time, with the AdS_2 metric written in Poincaré coordinates.

As we will see later in this paper, the extremal solution is a zero-temperature, zero-entropy solution. The extremal configuration will be then thermodynamically preferred. Even if a solution with two horizons could result from astrophysical collapse of a compact object, it will decay in a time much shorter than the Hawking evaporation time into the extremal configuration.

Let us conclude this subsection by noting that the extremal solution is stabilized by a particular profile for the energy density ϵ and for the pressures $p_\parallel$ and $p_\perp$. In the near-horizon approximation, when the metric takes the simple $AdS_2 \times S^2$ form, we expect them to be constant and to satisfy a simple EoS. In fact, combining Eqs. (5c), (6) and (22), the extremality conditions (25) and the EoS (9), we find that the leading terms for the near-horizon energy density and pressures are

$$\epsilon^{(\mathrm{nh})} = \frac{1}{8\pi G r_c^2}, \qquad p_\parallel^{(\mathrm{nh})} = -\epsilon^{(\mathrm{nh})}, \tag{29a}$$

$$\epsilon_{(\mathrm{AdS})}^{(\mathrm{nh})} = -\frac{1}{8\pi G L_2^2}, \qquad p_\perp^{(\mathrm{nh})} = -\epsilon_{(\mathrm{AdS})}^{(\mathrm{nh})}, \tag{29b}$$

where $\epsilon_{(\mathrm{AdS})}^{(\mathrm{nh})}$ is the (negative) constant energy density sourcing AdS_2. It is quite interesting to note that both

the radial and perpendicular components of the pressure satisfy the simple equation of state $p = -\epsilon$. The (positive) energy density associated to the two-sphere acts as a source for the (negative) radial pressure, whereas the (negative) energy density associated to AdS_2 acts as source for the (positive) perpendicular pressure. Thus, the stabilization of the $AdS_2 \times S^2$ near-horizon, extremal solution is achieved in a rather nontrivial way.

C. Black hole thermodynamics

From the metric function (22), using standard formulas, we can compute both the Hawking temperature T_H and the black-hole mass for the quantum corrected black hole, as functions of the outer horizon radius $r_+ \equiv r_H$ and of quantum deformation parameter ℓ:

$$T_H(r_H, \ell) = \frac{1}{4\pi}\frac{dA(r)}{dr}\bigg|_{r=r_H} = -\frac{\alpha}{4\pi\ell}F'\bigg|_{y=y_H},$$
$$M(r_H, \ell) = \frac{\ell}{2G}F^{-1}(y_H). \tag{30}$$

An important point is that ℓ has to be considered as a quantum-deformation parameter which, contrary to M, is not associated with conserved charges. This makes our quantum black-hole solution drastically different from other two-parameter classes of solutions, like, e.g., the charged RN solution, for which *both* parameters are associated with thermodynamic potentials.

Owing to this feature, we look for a first law of thermodynamics of the form $dM = T_H dS$, where S is the black hole entropy. One can easily check that the area law, i.e., an entropy equal to a quarter of the area of the outer event horizon (in Planck units), cannot be valid for our class of black-hole models. In fact, using $S_A = \mathcal{A}_H/4G = \pi r_H^2/G$, we get $dM - T_H dS_A = -(1/2G)(dF/dy_H)F^{-1}(F^{-1} - r_H/\ell)dr_H$. This tells us that, once the area law is assumed, the first principle is satisfied only for $F(y) = \ell/r_H$, i.e., only for the Schwarzschild black hole.

Let us now look for a new definition of the black hole entropy S, generalizing the area law, such that the first principle is satisfied. This generalized entropy can be found by noticing that Eq. (30) implies the validity of the following relation

$$dM = 4\pi M T_H dr_H. \tag{31}$$

By defining the black hole entropy as

$$S = 4\pi \int M dr_H, \tag{32}$$

we see that the first principle $dM = TdS$ is satisfied. Moreover, the entropy (32) correctly reproduces the area law in the Schwarzschild case, $M = r_H/2G$. Equation (32) defines the entropy of the hole up to an integration constant, which can be fixed by requiring the entropy area law to be recovered in the limit $\ell \ll R_S$, i.e., in the classical limit of our quantum model. This leads to

$$S(r_H) = 4\pi \int_{r_m}^{r_H} M(r'_H) dr'_H, \tag{33}$$

where r_m is the minimum value of the horizon radius. In the limit $\ell \ll R_S$, we have $M(r_H) = r_H/2G$ and $r_m = 0$, so that Eq. (33) gives the area law $S = \pi r_H^2/G$.

For a generic quantum deformed black hole, r_m is given by the radius r_c of the extremal black hole. This implies in particular that the extremal black hole has zero entropy, i.e., $S(r_c) = 0$. The extremal limit for our quantum deformed black hole is therefore a state of nonvanishing mass, but with zero temperature and entropy. Again, this behavior is drastically different from that of usual extremal black holes, for which the extremal configuration is a state with $T = 0$, but with $S \neq 0$.

Both for large black-hole radii $r_H \to \infty$ and in the extremal limit, the temperature goes to zero. This can be easily checked using Eq. (30) together with Eq. (24) and Eq. (25). Smoothness of the function $F(y)$ then implies that the function $T_H(r_H)$ has at least one local maximum in the range $[r_c, \infty)$. In order to avoid an oscillating behavior of $T_H(r_H)$, we have restricted ourselves to the simplest case by imposing condition 4 on the form of the function F (see the beginning of Sec. IV).

The temperature starts form zero in the extremal limit, then it reaches a maximum $T_{H,max}$ for $r_{H,max}$ and then goes down to zero again for large values of r_H/ℓ. This implies that T_H is always bounded, $0 \leq T_H \leq T_{H,max}$. Only when we take the limit $\ell \to 0$ first, to recover the Schwarzschild black hole, can the temperature become arbitrarily large by taking small black holes, $r_H \to 0$. Notice that a nonvanishing quantum deformation parameter, $\ell \neq 0$ solves, as expected, the singular thermodynamical behavior $T_H \to \infty$ of the Schwarzschild black hole for $r_H \to 0$. The typical qualitative behavior of the temperature is shown in Fig. 2.

In order to study in detail the thermodynamic behavior of the black hole near extremality, we expand T_H and M near r_c. At leading order, we get $T_H = \gamma(r_H - r_c)$, whereas $M = M_c + \beta(r_H - r_c)^2$, where $\gamma = dT_H/dr_H|_{r_c}$, $\beta = (1/2)d^2M/dr_H^2|_{r_c}$ and $M_c = M(r_c)$. Notice that dM/dr_H is always positive and becomes zero at extremality, $dM/dr_H|_{r_c} = 0$. For this reason, the linear term in the expansion of M is absent. The previous expression implies a quadratic scaling with the temperature of the mass above extremality

$$M - M_c \sim \frac{\ell^3}{G}T_H^2, \tag{34}$$

which is fully consistent with the $AdS_2 \times S^2$ near-horizon behavior of the extremal limit [121–123]. This means that, in

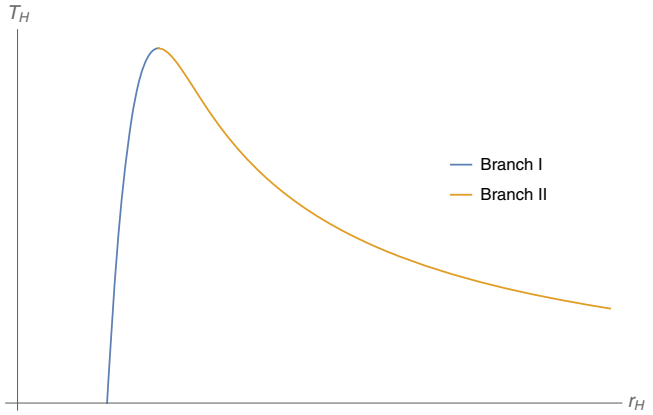

FIG. 2. Typical qualitative behavior of the black hole temperature $T_{\rm H}$ as a function of the black hole radius $r_{\rm H}$. We explicitly show the presence of the two branches.

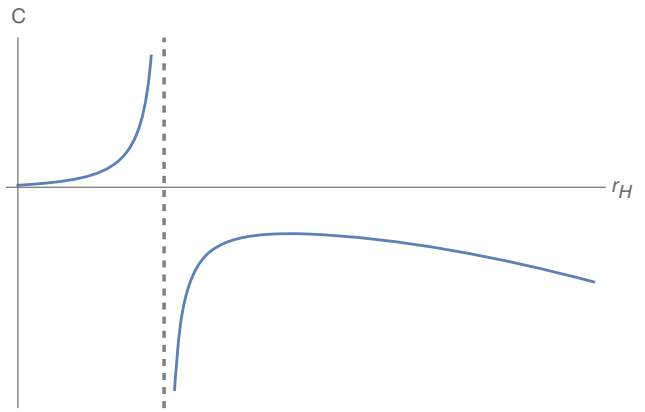

FIG. 3. Typical qualitative behavior of the black hole specific heat C as a function of $r_{\rm H}$. The $r_{\rm H}$-axis starts from the value at which C is zero, i.e., at the extremal value of $r_{\rm H}$, given by the solution of Eq. (25). The vertical dashed line, where C diverges, corresponds to the zero of $dT/dr_{\rm H}$, i.e., the maximum of the temperature.

the near-extremal limit, the black hole allows for an effective description in terms of a 2D dilaton gravity theory, i.e., Jackiw-Teitelboim (JT) gravity, with the dilaton parametrizing the radius of the 2-sphere S^2 [124–126]. This in turn implies the possibility of using a dual 2D conformal field theory to describe the near-horizon regime of the near-extremal black hole. This fact may be relevant for applications to the information puzzle in black-hole physics [34,35,65–69].

D. Phase transition

The nonmonotonic behavior of $T(r_{\rm H})$, which is common to a wide class of charged and/or AdS black holes, signalizes a nontrivial thermodynamic phase structure, the presence of two thermodynamic branches and a phase transition at the critical temperature $T_{\rm H,max}$ (see, e.g., Refs. [127–136]). This simply follows from the fact that we have two possible values of $r_{\rm H}$ for a given value of $T_{\rm H}$. This implies the presence of metastable states and the existence of two branches, I and II. Branch I corresponds to small, order 1 values of the dimensionless black hole radius $y_{\rm H}$ (the left-hand region of Fig. 2). In this branch, $r_{\rm H}$ varies between the extremal value r_c and $r_{\rm H,max}$. Correspondingly, the parameter ℓ takes values between $\ell_{\rm H,max}$ and ℓ_c, both of order $R_{\rm S}$. Thus, branch I describes quantum black holes whose quantum deformation parameter ℓ is of the same order of magnitude of the classical Schwarzschild radius $R_{\rm S}$. Conversely, branch II corresponds to large values of $y_{\rm H}$ (the right-hand region of Fig. 2). Here, $r_{\rm H}$ can take values much larger than $r_{\rm H,max}$. This corresponds to small values of the parameter ℓ. Thus, the far right region of branch II describes classical black holes, with quantum deformation parameter $\ell \ll R_{\rm S}$.

The phase transition and the stability of the different thermodynamic phases can be investigated by considering the specific heat of the black hole:

$$C = \frac{dM}{dT} = \frac{dM}{dr_{\rm H}}\left(\frac{dT}{dr_{\rm H}}\right)^{-1}. \tag{35}$$

Being $dM/dr_{\rm H}$ always positive, the nonmonotonic behavior of $T_{\rm H}$ implies that

(i) For $r_c < r_{\rm H} < r_{\rm H,max}$, $dT/dr_{\rm H}$ is positive and thus $C > 0$;
(ii) For $r_{\rm H} > r_{\rm H,max}$, $dT/dr_{\rm H}$ is negative and thus $C < 0$;
(iii) For $r_{\rm H} = r_{\rm H,max}$, $dT/dr_{\rm H} = 0$ and thus $C \to \infty$.

In Fig. 3 we plot the qualitative behavior of the specific heat C as a function of $r_{\rm H}$.

In branch I, i.e., for values of $r_{\rm H}$ less than $r_{\rm H,max}$, the specific heat is always positive and the black hole exists in equilibrium with its radiation. On the other hand in branch II, i.e., for values of $r_{\rm H}$ larger than $r_{\rm H,max}$, the specific heat is always negative and the black hole cannot be considered at equilibrium with its radiation anymore. A second order phase transition occurs at $r_{\rm H,max}$. This implies that quantum black holes with small values of the quantum deformation parameter are thermodynamically less favored with respect to black holes with $\ell \sim R_{\rm S}$. Moreover, the value of the deformation parameter ℓ at the maximum, $\ell_{\rm H,max}$, is very close to the extremal value. This means that black holes close to extremality are thermodynamically preferred, which further confirms the choice $\ell \sim GM$. This also shows that the outcome of the evaporation process will be a *cold* remnant at zero temperature and zero entropy. The latter, in particular, is again an intriguing property, as it could allow to circumvent problems on the viability of remnants as possible solutions on the information paradox [137].

These thermodynamic aspects and the phase picture will be confirmed later on this paper, when we will consider particular cases of our general class of models and we will study their free energy.

The nontrivial phase space structure analyzed above is a consequence of the multiscale description of our models, discussed in Sec. II. In light of the similarity between this description of gravitational interactions and glassy systems [44], one could ask whether our phase transition could be interpreted as a glass transition. Indeed, even the latter is characterized by a divergence in the specific heat at the transition point, but it is not generally classified as a second-order phase transition. To answer this question, one would need first to define some Ehrenfest equations, to describe variations of the specific heat and the derivatives of the volume between the two phases. For a second-order phase transition, both these equations are satisfied, while either both or one of them is violated in glassy systems. In the black-hole case, one can define Ehrenfest-like equations [138] by replacing the volume with the electric charge and/or the angular momentum (if the model is charged and/or rotating) and analyze their variations between the two phases.

Here, we can only speculate that the phase transition of our "quantum-corrected" black hole could be very similar to a glass transition instead of a second-order one. In fact, the absence of any thermodynamic potentials related to ℓ or other physical observables prevents us from properly defining Ehrenfest-like equations, and therefore to perform an analysis similar to the one in Ref. [138]. Consequently, this does not allow us to assess quantitatively the nature of the phase transition in our models.

Summarizing the results obtained so far, the stable configuration of our quantum-black-hole model, realized using an anisotropic fluid, will be represented by an extremal (or near-extremal, if we consider small deviations from extremality) black hole. The black-hole geometry interpolates between a dS space-time in the black-hole interior (near the singularity), an $AdS_2 \times S^2$ geometry in the near-horizon region, and flat space-time in the asymptotic, $r \to \infty$, region. The dS behavior near $r = 0$ solves the singularity problem. At extremality, the two (dual) quantum scales characterizing the quantum black hole (ℓ, $\hat{L}$) have the same order of magnitude of the classical black-hole radius R_S.

The scale ℓ characterizing quantum effects seen by an external observer is naturally of the order of magnitude of the classical Schwarzschild radius R_S of the black hole. This opens the possibility of having phenomenological quantum signatures, potentially observable in the near future, e.g.. through the QNMs spectrum and the geodesic motion of particles near the horizon. Moreover, the near-horizon $AdS_2 \times S^2$ behavior is very promising for tackling the black-hole information puzzle.

E. Null geodesics and photon orbits

To compute photon orbits in our class of models, we start from the geodesic equation together with the null-geodesic constraint (dot will refer to derivation with respect to the affine parameter)

$$\ddot{x}^\mu + \Gamma^\mu_{\nu\lambda}\dot{x}^\nu\dot{x}^\lambda = 0, \qquad g_{\mu\nu}\dot{x}^\mu\dot{x}^\nu = 0. \tag{36}$$

The isometries of the metric (spherical symmetry and invariance under time translations) imply two conservation equations, which by considering geodesics on the plane $\theta = \text{constant} = \pi/2$, take the form

$$\dot{\phi} = \frac{J}{r^2}, \qquad \dot{t} = \frac{\mathcal{C}}{|A(r)|} \tag{37}$$

where J and $\mathcal{C}$ are integration constants.

The geodesic equation for the coordinate r can be integrated to give,

$$\dot{r}^2 + \frac{J^2}{r^2}A(r) = \mathcal{C}^2, \tag{38}$$

which can be rewritten as the energy conservation equation:

$$\frac{1}{2}\dot{r}^2 + V(r) = \frac{\mathcal{C}^2}{2} \equiv \mathcal{E}, \tag{39}$$

with $\mathcal{E}$ a constant and $V(r)$ the effective potential

$$V(r) \equiv \frac{J^2}{2r^2}A(r). \tag{40}$$

Since the leading term of metric function for $r \to 0$ is $A(r) \sim 1$, we have $V(r) \to \infty$ in this limit. This behavior is completely different from the Schwarzschild case ($V \to -\infty$ as $r \to 0$) and is a consequence of the absence of a singularity. Conversely, for $r \to \infty$, $A(r)$ is dominated by the $1/r$ term and $V(r) \to 0$, as in the Schwarzschild case. The shape of the effective potential $V(r)$ at intermediate distances depends crucially on the values of the parameter α. The local extrema of V are the solution of the equation

$$rA'(r) - 2A(r) = 2\alpha F - 2 - \frac{\alpha r}{\ell}F' = 0. \tag{41}$$

Being F and F' both bounded, it will always exist a minimum value $\alpha_m < \alpha_c$ such that for $\alpha \leq \alpha_m$ the equation has no (real) zeroes and bounded photon orbits do not exist. For $\alpha > \alpha_m$, the equation allows instead for two (real) zeroes, corresponding to a local minimum and a local maximum for $V(r)$. On the other hand, for $\alpha_m < \alpha < \alpha_c$, we still have the stable and unstable photon orbits, but there are no horizons, since the solution describes a star. For $\alpha = \alpha_c$, i.e., in the extremal configuration, the minimum of the potential coincides with the horizon position. In this case, we will have both the outer unstable photon ring and a stable one, which, however, coincides with the event horizon of the extremal black hole. Finally, for $\alpha > \alpha_c$, the local minimum is inside the event horizon and we have only a bounded unstable photon orbit, similarly to the Schwarzschild case.

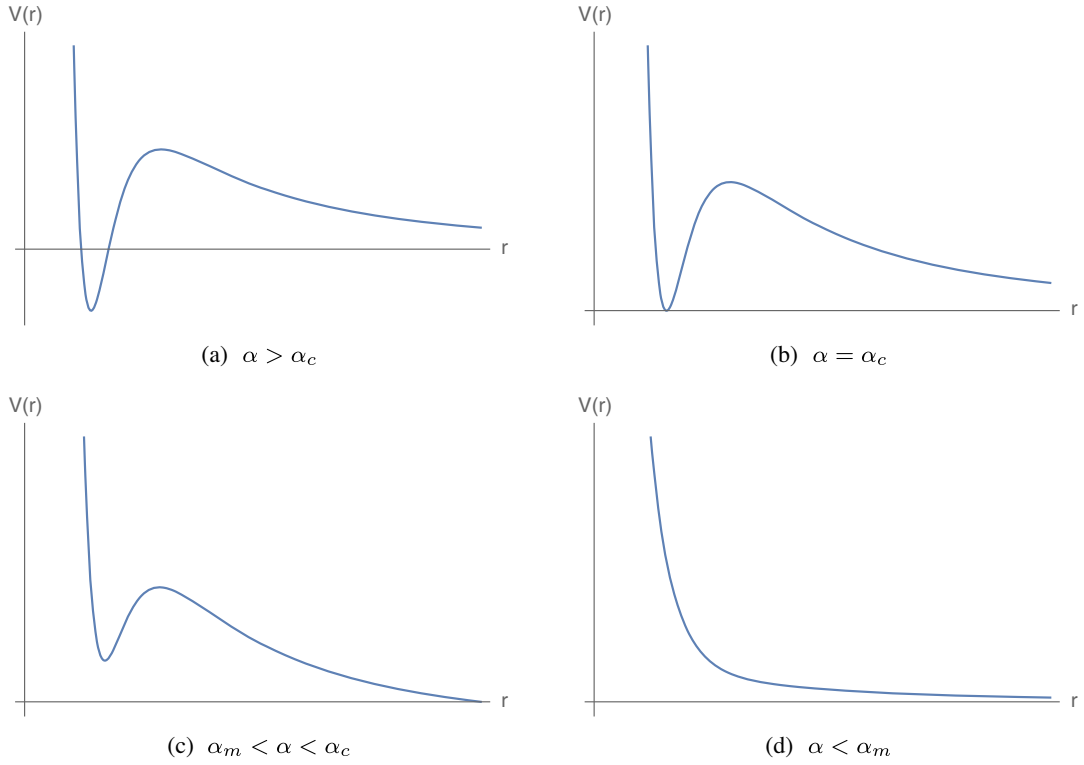

FIG. 4. Typical qualitative behavior of the effective potential V for null geodesics as a function of r for $\alpha > \alpha_c$, $\alpha = \alpha_c$, $\alpha_m < \alpha < \alpha_c$ and $\alpha < \alpha_m$.

The qualitative behavior of $V(r)$ in the four cases is shown in Fig. 4. From the plots we see that there are two main differences with the Schwarzschild case. The first is the possibility of having a complete absence of bounded orbits, in the case of the horizonless solution. The second is the presence of stable orbits for photons in addition to the usual unstable ones. However, in the two-horizon case, the stable orbits are beyond the black-hole horizon and do not play any role, while in the extremal case they coincide with the horizon. Deviations from extremality, however, push this minimum inside the outer horizon and their effects are irrelevant from the observational point of view.

F. Quasinormal modes spectrum in the eikonal approximation

In this section we consider QNMs for scalar perturbations in the fixed background given by our general black-hole solution. We will then use the eikonal approximation to give an analytical estimate of the quasinormal frequencies.

The evolution of scalar perturbations Ψ, in the fixed gravitational background metric $g^{(B)}_{\mu\nu}$ described by the metric function (22), is determined by the Klein-Gordon equation

$$\Box\Psi = \frac{1}{\sqrt{-g^{(B)}}}\partial_\mu\left(\sqrt{-g^{(B)}}g^{\mu\nu}_{(B)}\partial_\nu\right)\Psi = 0. \tag{42}$$

By separating the time, angular and radial parts of Ψ, one gets the radial Schrödinger-like equation for the r-dependent part,

$$\frac{d^2\psi}{dr_*^2} + [\omega^2 - V_{\rm KG}(r)]\psi = 0, \tag{43}$$

where the potential is

$$V_{\rm KG}(r) = (1-\alpha F)\left[\frac{l(l+1)}{r^2} - \alpha\frac{F'}{\ell' r}\right], \tag{44}$$

l is the orbital-angular-momentum number and r_* is the tortoise coordinate defined by

$$r_* = \int \frac{dr}{A(r)}. \tag{45}$$

Analytical estimates of the quasinormal frequencies can be obtained by using an intriguing relation between quasinormal modes and the parameters characterizing null geodesics in the eikonal limit $l \gg 1$ first noted in Ref. [139]. The vibration modes of the black holes, whose energy is gradually being radiated away, are interpreted as photons moving along an unstable null-geodesics and slowly leaking out. This correspondence was more recently analyzed in Refs. [140–142] and shown to agree with WKB results [143,144]. Specifically, the angular velocity

$\Omega_m = \dot{\varphi}/\dot{t}|_{r=r_m}$, computed at the maximum of the geodesic potential r_m, determines the real part of the quasinormal spectrum. Further, the so-called Lyapunov exponent $\lambda = \sqrt{\frac{V''(r)}{2\dot{t}^2}}|_{r=r_m}$ [$V(r)$ is the effective potential for null geodesics (40)], which characterizes the timescale of the null-orbit instability, describes the damping of the black hole oscillations and therefore determines the imaginary part of the spectrum. We have

$$\omega_{\rm QNM} = \omega_{\rm R} + i\omega_{\rm I} = \Omega_m l - \mathrm{i}\left(n + \frac{1}{2}\right)|\lambda|, \tag{46}$$

where

$$\Omega_m = \sqrt{\frac{A'(r)}{2r}}\bigg|_{r=r_m} = \frac{\sqrt{A(r_m)}}{r_m}; \tag{47a}$$

$$\lambda = \frac{1}{\sqrt{2}}\sqrt{-\frac{r_m^2}{A(r_m)}\left(\frac{d^2}{dr_*^2}\frac{A(r)}{r^2}\right)_{r=r_m}}. \tag{47b}$$

Being r_m the position of the peak of the geodesic potential, it is given by the solution of the Eq. (41). Although we have seen that, for extremal black holes, the potential V has an additional minimum exactly at the horizon, we will not consider this contribution, as small perturbations from extremality have the effect of moving this minimum toward the black hole interior. The QNMs spectrum will be therefore entirely determined by the contribution at the maximum of V.

The general expressions (47a) and (47b) are valid for all spherically-symmetric, static and asymptotically-flat solutions, in the eikonal limit. For our general class of models, using Eqs. (22), (45), (47a) and (47b) we get

$$\omega_{\rm R} = \frac{l}{r_m}\sqrt{A(r_m)} = \frac{l}{\ell y_m}\sqrt{1-\alpha F_m}, \tag{48a}$$

$$\begin{aligned}\omega_{\rm I} &= -\left(n+\frac{1}{2}\right)\frac{1}{\sqrt{2}}\sqrt{A(r_m)r_m\left|\left(\frac{A'(r)}{r}\right)'_m\right|} \\ &= -\left(n+\frac{1}{2}\right)\frac{1}{\sqrt{2}\ell}\sqrt{\alpha(1-\alpha F_m)y_m\left|\left(\frac{F'}{y}\right)'_m\right|}.\end{aligned} \tag{48b}$$

It is important to stress that the QNMs frequencies depend both from the classical hair M and from the quantum hair ℓ. This dependence from two parameters of the QNMs spectrum will have a well-defined signature in the ringdown part of the gravitational wave generated in the merging of two compact objects to form a single black hole. Next-generation gravitational-wave detectors are expected to be sensitive enough to detect such effect.

In the generic case, $\omega_{\rm R}$ and $\omega_{\rm I}$ will be complicated functions of α. Simpler expressions can be obtained for near-extremal black holes, by expanding in powers of $(\alpha - \alpha_c)$. Taking into account that $|A|_m \neq 0$ (see the remark above), if we just consider the near-extremal expansion but not the near-horizon expansion, we will also have $(\frac{A(r)'}{r})'_m \neq 0$. At first order in $(\alpha - \alpha_c)$ we get $\omega_{\rm I} = \text{constant}/\ell + \text{constant}(G/\ell^2)(M - M_c)$ and similarly for $\omega_{\rm R}$. Using Eq. (34), we can express the quasinormal frequencies in terms of the black hole temperature

$$\omega_{\rm R} = \frac{a}{\ell} + b\ell T_{\rm H}^2, \tag{49a}$$

$$\omega_{\rm I} = \frac{c}{\ell} + d\ell T_{\rm H}^2, \tag{49b}$$

where a, b, c, d are dimensionless constants.

On the other hand, if we take the near-horizon limit together with the near-extremal limit, the metric satisfies $(\frac{A(r)'}{r})' = 0$, identically, since the geometry becomes that of $\mathrm{AdS}_2 \times \mathrm{S}^2$. While the behavior of $\omega_{\rm R}$ remains that of Eq. (49), we get a linear scaling of $\omega_{\rm I}$ with the temperature, owing to the absence of the constant term inside the square root:

$$\omega_{\rm I} \propto T_{\rm H}. \tag{50}$$

These results confirm only partially Hod's conjecture, which asserts the complete absence of the imaginary damped part in the spectrum in the near-extremal case, both for RN and Kerr black holes [75–79]. In the case under consideration, Hod's conjecture seems to hold true only in the near-extremal, near-horizon case. This seems to be a feature of also general charged and rotating regular black-hole models [82–84].

On the other hand, our results seem to confirm a general behavior found in Ref. [145] for the near-extremal Kerr space-time, which is characterized by a branching in the quasinormal spectrum. One family, corresponding to the simple near-extremal limit, has indeed a nonvanishing imaginary part in the extremal limit, while the other branch shows that the damped part of the spectrum goes to zero in the near-extremal, near-horizon limit.

Finally, the temperature scaling (50) fully confirms previous derivation of the quasinormal spectrum for two dimensional AdS_2 black holes [70–74]. In fact, the latter allows for an explicit *analytical* treatment through different methods, which all point toward the same result: a linear scaling of the imaginary part $\omega_{\rm I}$ with the temperature of the hole. A quite interesting consequence of this scaling is the complete absence of the imaginary damped part in the spectrum in the extremal case, as the temperature becomes zero. These zero-damped (or nearly zero-damped) modes [75–81] would therefore represent a clear phenomenological signature of extremal black holes.

V. A MINIMAL MODEL: THE HAYWARD BLACK HOLE

The simplest example of our general class of models is given by the Hayward black-hole metric [94,146], for which the metric function F in Eq. (22) reads

$$F(y) = \frac{y^2}{y^3+1}, \tag{51}$$

with $y \geq 0$. As already mentioned in Sec. IV, the analysis of Ref. [116] shows that an algebraic form of F could be inconsistent with semiclassical field equations derived from an action principle, at least if one requires the solutions to be derived from an Einstein-Hilbert action with higher-order terms in the curvature.

The horizon location and the extremality condition (25) are now

$$y^3 - \alpha y^2 + 1 = 0, \qquad -2\alpha y + 3y^2 = 0. \tag{52}$$

Solving these equations yields the critical values of the parameter α and the critical radius r_c

$$\alpha_c = \frac{3}{\sqrt[3]{4}}, \qquad r_c = \frac{2}{3}R_{\rm S} = \sqrt[3]{2}\ell. \tag{53}$$

The black hole has two horizons for $R_{\rm S} > 3\ell/\sqrt[3]{4}$, is extremal for $R_{\rm S} = 3\ell/\sqrt[3]{4}$, whereas it becomes a horizonless star for $R_{\rm S} < 3\ell/\sqrt[3]{4}$. The energy density ϵ and the mass function m sourcing the black hole are given by

$$\epsilon(r) = \frac{3}{4\pi}\frac{M\ell^3}{(r^3+\ell^3)^2}, \qquad m(r) = \frac{Mr^3}{r^3+\ell^3}. \tag{54}$$

The NEC (12) is always satisfied, while the SEC (13) is violated deep inside the core of the object, for $r \leq \ell/\sqrt[3]{2}$. On the other hand, for $\ell \to 0$, or for $r \to \infty$, $\epsilon(r)$ has a very small, Dirac's delta-like support only in the region near $r = 0$, and therefore $m(r) = M$: the Schwarzschild black hole is recovered. The deviation from the Schwarzschild case can be characterized by defining a mass deviation $\Delta m(r)$ as the difference between the mass at infinity M and $m(r)$, which in the present case reads

$$\Delta m \equiv M - m(r) = \frac{M\ell^3}{r^3+\ell^3}. \tag{55}$$

For $r \to \infty$, it behaves as

$$\Delta m \sim \frac{M\ell^3}{r^3} + \mathcal{O}\left(\frac{1}{r^4}\right). \tag{56}$$

The solution is asymptotically flat and satisfies the boundary conditions ϵ, $p_\parallel$, $p_\perp \to 0$ for $r \to \infty$, while it has a dS behavior near $r = 0$ with the dS length $\hat{L}$ (15) given by

$$\hat{L} = \ell^{3/2} R_{\rm S}^{-1/2}, \tag{57}$$

which relates ℓ with the Schwarzschild radius and the dS length characterizing the small r behavior. Equation (57) fully confirms the validity of our general scaling given by Eq. (19).

We note that the same result in Eq. (57) can be obtained in the limit of very large ℓ. In this case, however, we have an *exact* solution of Einstein's equations, sourced by a constant-density, *isotropic* and *homogeneous* fluid, with equation of state

$$p_\parallel = p_\perp = -\epsilon = -\frac{3}{8\pi G\hat{L}^2}. \tag{58}$$

Indeed, looking at the density profile (51), the dS universe can be recovered in the limit $\ell \to \infty$ only if $M \to \infty$, so that the energy density of the source (51) becomes constant.

For $\alpha > \alpha_c$, the cubic equation in (53) has three real roots, out of which two are positive, r_+ and r_-, denoting the outer and inner horizons respectively, whereas the third, r_3, is negative. The metric function A factorizes as

$$A(r) = \frac{(r-r_+)(r-r_-)(r-r_3)}{r^3+\ell^3}. \tag{59}$$

In the extremal limit $r_+ = r_- \equiv r_c = (2/3)R_{\rm S}$, after a translation of the radial coordinate $r \to r + r_c$, the space-time metric becomes

$$\begin{aligned} ds^2 &= -\tilde{A}(r)dt^2 + \tilde{A}^{-1}(r)dr^2 + (r+r_c)^2 d\Omega^2, \\ \tilde{A}(r) &\equiv \frac{r^2(r+r_c-r_3)}{(r+r_c)^3+\ell^3}, \end{aligned} \tag{60}$$

describing an asymptotically flat region connected with an infinitely long throat of radius r_c. The near horizon (around $r = 0$) expansion of the metric (60) gives the $\mathrm{AdS}_2 \times \mathrm{S}^2$ space-time (27), with an AdS_2 length $L_2 = (2/3)R_{\rm S}$. The fluid stabilizing the extremal solution is characterized by the equations of state (29), where now the AdS_2 length L_2 and the radius r_c of the two-sphere have the same value, $L_2 = r_c = (2/3)R_{\rm S}$.

A. Thermodynamics and phase transition

Inserting F given by Eq. (51) into Eq. (30), we get the mass and temperature of the black hole

$$T_{\rm H} = \frac{1}{4\pi r_{\rm H}}\frac{r_{\rm H}^3 - 2\ell^3}{r_{\rm H}^3+\ell^3}, \qquad M = \frac{1}{2G}\left(r_{\rm H} + \frac{\ell^3}{r_{\rm H}^2}\right). \tag{61}$$

The temperature behavior agrees with the expected qualitative one shown in Fig. 2. The maximum of $T_{\rm H}$ is

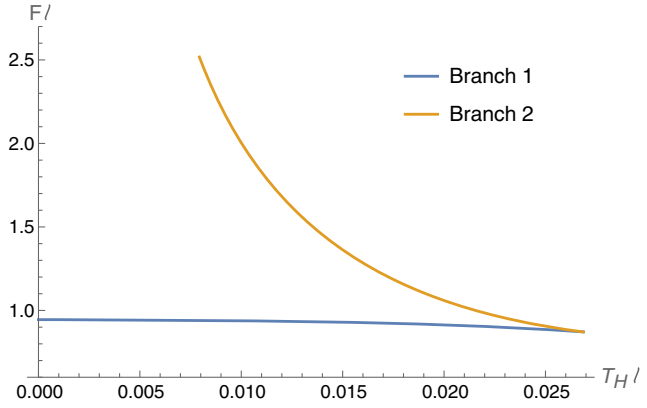

FIG. 5. Free energy $\mathcal{F}$, in units of ℓ^{-1}, as a function of the temperature, in units of ℓ^{-1}, for the two branches of the Hayward black hole. We plot $\mathcal{F}$ for branch I, $\ell \sim R_S$ (solid blue curve), and for branch II (solid orange curve) corresponding to $\ell \ll R_S$. We see that "quantum deformed" black holes with $\ell \sim R_S$ are always energetically preferred with respect to those with $\ell \ll R_S$.

obtained by solving the equation $y^6 - 10y^3 - 2 = 0$, giving $r_H = \sqrt[3]{(5+3\sqrt{3})}\ell$.

Expanding Eq. (61) near extremality, one easily finds the quadratic scaling (34) of the mass with the temperature

$$M - M_c = 12\pi^2 \frac{\ell^3}{G} T_H^2. \tag{62}$$

The black-hole entropy satisfying the first principle of thermodynamics is easily obtained from Eq. (32)

$$S = \frac{\pi r_H^2}{G} - \frac{2\pi\ell^3}{G r_H} \tag{63}$$

The first term is the standard area law, while the second term describes ℓ-dependent deviations.

The specific heat C can easily be calculated using Eq. (61) and agrees with the qualitative behavior shown in Fig. 3. It diverges for $r_H = \sqrt[3]{(5+3\sqrt{3})}\ell$, indicating the onset of the second order phase transition, with the stable thermodynamic branch I occurring for $r_H < \sqrt[3]{(5+3\sqrt{3})}\ell$.[5]

The existence of this phase transition and related thermodynamical phase portrait can be checked by computing the free energy $\mathcal{F} = M - T_H S$ as a function of the temperature. The free energy for the two branches I and II has to be calculated numerically by inverting the equation $T_H = T_H(r_H)$. We plot $\mathcal{F}(T_H)$ in Fig. 5. Branch I corresponds to r_H varying between the extremal value r_c and $r_{H,max}$, and thus it describes quantum black holes for which the quantum deformation parameter ℓ is of the same order of magnitude of the classical Schwarzschild radius R_S. Conversely, branch II corresponds to r_H taking values much larger than $r_{H,max}$, where $\ell \ll R_S$, corresponding to the classical black-hole branch.

We note that the branch I is always energetically preferred with respect to branch II, which further supports our choice $\ell \sim R_S$.

[5]The possibility of having a phase transition in the Hayward model has been previously recognized in Ref. [147].

B. Null geodesics and quasinormal modes in the eikonal limit

Let us now consider geodesic motion and QNMs for the Hayward black hole. The effective potential (40), which determines photon orbits in the black-hole background, in the present case reads

$$V(r) = \frac{J^2}{2r^2}\left(1 - \frac{R_S r^2}{r^3 + \ell^3}\right). \tag{64}$$

The extrema of $V(r)$ are determined by Eq. (41) with A given by Eq. (59), i.e., by the roots of the equation $2y^6 - 3\alpha y^5 + 4y^3 + 2 = 0$. By solving this equation numerically, one can show that no real roots exist for $\alpha < \alpha_m \approx 1.64$. The position of the maximum of the potential will depend on the value of the parameter α with respect to α_m and $\alpha_c = 3/\sqrt[3]{4}$. Also here, we can distinguish between the four cases shown in Fig. 4. The quasinormal frequencies in the eikonal approximation for the Hayward black-hole can be easily calculated plugging Eq. (51) into Eqs. (48a) and (48b). One has

$$\omega_R = \frac{l}{\ell y_m}\sqrt{1 - \alpha\frac{y_m^2}{y_m^3+1}},$$
$$\omega_I = -\left(n+\frac{1}{2}\right)\frac{\sqrt{3\alpha}y_m^{3/2}}{\sqrt{2}\ell(1+y_m)^2}\sqrt{|y_m^3-5|(1+y_m^3-\alpha y_m^2)}. \tag{65}$$

By expanding around $\alpha = \alpha_c = 3/\sqrt[3]{4}$, we get

$$\omega_R \simeq \frac{0.21l}{\ell} - \frac{0.11l}{\ell}(\alpha - \alpha_c) \simeq \frac{0.21l}{\ell} - 26.13 l\ell T_H^2; \tag{66a}$$

$$\omega_I \simeq -\left(n+\frac{1}{2}\right)\frac{5.70}{\ell} + \left(n+\frac{1}{2}\right)\frac{1.44}{\ell}(\alpha - \alpha_c)$$
$$\simeq -\left(n+\frac{1}{2}\right)\frac{5.71}{\ell} + \left(n+\frac{1}{2}\right)340.07\ell T_H^2, \tag{66b}$$

where in the last equalities we used the definition of α and Eq. (62).

VI. QUANTUM BLACK HOLES WITH GAUSSIAN CORES

Another explicit and simple realization of a regular quantum black hole, sourced by an anisotropic fluid with EoS given by Eq. (9) and satisfying the conditions outlined in Sec. IV, can be obtained by taking a Gaussian density distribution in the interior of the astrophysical object, peaked at $r = 0$

$$\epsilon(r) = \frac{M}{\pi^{3/2}\ell^3} e^{-r^2/\ell^2}, \tag{67}$$

where M is the MS mass as seen from infinity, namely

$$M = 4\pi \int_0^\infty dr r^2 \epsilon(r). \tag{68}$$

The parameter ℓ represents here a smearing of the classical Schwarzschild-Dirac delta-density profile (the latter is recovered in the limit $\ell \to 0$). Such a density profile is motivated by several microscopic descriptions of black holes: noncommutative geometry [22,148], loop quantum gravity (LQG) [26], corpuscular picture [149]. The NEC condition (12) is always satisfied, while the SEC (13) is again violated in the deep core of the body, i.e., for $r < \ell$.

Near $r = 0$, the space-time behaves as dS, with a dS length $\hat{L}$ given by

$$\hat{L} = \sqrt{\frac{3}{4}} \pi^{1/4} \ell^{3/2} R_S^{-1/2}, \tag{69}$$

confirming again our general result given by Eq. (19).

As we also saw in Sec. V, the same result can be obtained as an exact solution of Einstein's field equations, sourced by the fluid with EoS (58), in the limit $\ell \to \infty$. Indeed, looking at the density profile (67), the dS universe can be recovered in the limit $\ell \to \infty$ only if $M \to \infty$, and the energy density (67) behaves as a constant.

Let us turn our attention to the metric structure, by computing the MS mass at a generic r

$$\begin{aligned} m(r) &= 4\pi \int_0^r d\tilde{r}\, \tilde{r}^2 \epsilon(\tilde{r}) = \frac{2M}{\sqrt{\pi}} \gamma\left(\frac{3}{2}, \frac{r^2}{\ell^2}\right) \\ &= M\left[1 - \frac{2}{\sqrt{\pi}} \Gamma\left(\frac{3}{2}, \frac{r^2}{\ell^2}\right)\right] \end{aligned} \tag{70}$$

where $\gamma(a,z) = \int_0^z dt e^{-t} t^{a-1}$ and $\Gamma(a,z) = \int_z^\infty dt e^{-t} t^{a-1}$ are the incomplete gamma functions. The first term in Eq. (70) is the mass measured at infinity (the Schwarzschild ADM mass), while the second term, parametrized by ℓ, encodes the quantum corrections, the effects of the smearing of the singularity. The deviation from the Schwarzschild solution, described by the mass deviation $\Delta m(r) \equiv M - m(r)$, is strongly suppressed outside the core of the compact object, as for $r \to \infty$ it behaves as

$$\Delta m \sim \frac{M}{\sqrt{\pi}} e^{-\frac{r^2}{\ell^2}} \left(\frac{\ell}{r} + \frac{2r}{\ell}\right) \tag{71}$$

which represents a stronger suppression with respect to that of the Hayward model [see Eq. (56)].

The metric components can be written in the form of Eq. (22) with the metric function $F(y)$ given by

$$F(y) = \frac{1}{y}\left[1 - \frac{2}{\sqrt{\pi}} \Gamma\left(\frac{3}{2}, y^2\right)\right]. \tag{72}$$

Contrary to the Hayward model, in the present case, the nonalgebraic form of F allows to circumvent the viability constraints of Ref. [116].

Given the form of the metric functions, the position of the horizon(s) and the parameters range discriminating between the two-, one- or no horizons cases have to be computed numerically. The two horizons merge and we have the extremal case when both equations in (25) are satisfied. This translates into the conditions:

$$1 - \frac{2GM}{y\ell} + \frac{4GM}{\ell\sqrt{\pi} y} \Gamma\left(\frac{3}{2}, y^2\right) = 0; \tag{73a}$$

$$1 - \frac{2}{\sqrt{\pi}} \Gamma\left(\frac{3}{2}, y^2\right) - \frac{4y^3}{\sqrt{\pi}} e^{-y^2} = 0. \tag{73b}$$

These equations need to be solved numerically.[6] The numerical solution of Eq. (73b) is $y_{\min} \simeq 1.51$, which means $r_{\min} \simeq 1.5\ell$. The range of parameter $\alpha = R_S \ell^{-1}$ discriminating between the aforementioned three cases therefore is

(i) *No horizons*: $A(y = y_{\min}) > 0$

$$\alpha < \frac{3}{2 - \frac{4}{\sqrt{\pi}} \Gamma\left(\frac{3}{2}, \frac{9}{4}\right)}. \tag{74}$$

(ii) *One horizon*: $A(y = y_{\min}) = 0$

$$\alpha = \frac{3}{2 - \frac{4}{\sqrt{\pi}} \Gamma\left(\frac{3}{2}, \frac{9}{4}\right)} \simeq 1.90. \tag{75}$$

(iii) *Two horizons*: $A(y = y_{\min}) > 0$

$$\alpha > \frac{3}{2 - \frac{4}{\sqrt{\pi}} \Gamma\left(\frac{3}{2}, \frac{9}{4}\right)}. \tag{76}$$

In this latter case, the outer horizon is an event horizon, while the inner one is a Cauchy horizon [148].

[6] We discard the simplest analytical solution, i.e., $r = 0$, since it is not a minimum.

We have therefore a critical value ℓ_c for the quantum parameter ℓ for which the two horizons merge and the quantum black hole becomes extremal

$$\ell_c \simeq 0.53 R_S, \tag{77}$$

which is close to the classical gravitational radius of the compact object. This critical value discriminates between the three classes of solutions. When ℓ is above, equal or below ℓ_c we have a solution with two, one or none horizons, correspondingly. ℓ_c, in turns, determines a critical value $\hat{L}_c$ for dS length through Eq. (69), which also turns out to be close to the classical Schwarzschild radius[7]:

$$\hat{L}_c \simeq 0.31 R_S. \tag{78}$$

The most interesting case is the extremal black hole, obtained for $\ell = \ell_c$ ($\hat{L} = \hat{L}_c$). As discussed in Sec. IV, in the extremal case the near-horizon geometry factorizes as $AdS_2 \times S^2$, with the AdS_2 length given by $L_2^{-1} = \sqrt{-\frac{1}{2}A(r_c)''}$. L_2 can be calculated first using Eqs. (73a) and (73b) to get

$$e^{-y^2(r_c)} = \frac{\sqrt{\pi}\ell}{4R_S y^2(r_c)}. \tag{79}$$

Using this equation together with Eqs. (70), (72), (73a) and (73b) enables us to find

$$-\frac{1}{2}A(r_c)'' \equiv \frac{1}{L_2^2} = \frac{1}{\ell^2} - \frac{1}{r_c^2}. \tag{80}$$

Using Eq. (77) and taking into account that $r_{\min} \simeq 1.5\ell \simeq 0.78 R_S$ we get

$$L_2 \simeq 0.70 R_S, \tag{81}$$

confirming the general result of Sec. IV, according to which both the radius of the two-sphere and the AdS_2 length are of order R_S.

As shown at the end of Sec. IV B, the extremal solution is stabilized by a particular profile for the energy density ϵ and for the pressures $p_\parallel$ and $p_\perp$, given by the expressions (29). In the present case, the negative energy density sourcing the AdS_2 space-time reads $\epsilon^{(nh)}_{(AdS)} \equiv -1/(8\pi G L_2^2) = -(1/8\pi G)(1/\ell^2 - 1/r_c^2)$.

[7]The fact that $\hat{L}_c < \ell_c$ is expected: the SEC is violated in the deep core of the object, namely for $r < \ell$. This is perfectly consistent with the fact that this energy condition is violated in a dS space-time.

A. Quantum black hole regimes

The parameter ℓ (or equivalently $\hat{L}$) controls the scale of quantum effects in our quantum black-hole model. In the usual, most conservative approach, which assumes quantum gravity effects to be relevant only at the Planck scale ℓ_P, ℓ is assumed to be of the same order of magnitude of ℓ_P. This assumption is surely justified when ℓ has an explicit origin in the microscopic description of gravity at the Planck scale. It is for instance the case of Refs. [22,26,148,149], where the Gaussian model, and the parameter ℓ in particular, parametrizes UV noncommutative [22] or LQG [26] effects.

However, this is not the case in those approaches, like the one followed in this paper, in which an IR quantum scale, hierarchically smaller than ℓ_P, is generated. Given the attention the model with $\ell \sim \ell_P$ received in the past [21–29,31], it is worthwhile to quantitatively compare the two different regimes (1) $\ell \sim \ell_P$ and (2) $\ell \sim R_S$ for the black-hole model with a Gaussian core, and analyze the possible impact on observable phenomenology in the two cases. Again, we remind that we are considering macroscopic black holes, i.e., $R_S \gg \ell_P$.

1. $\ell \sim \ell_P$

In this case, Eq. (76) tells us that we always have two horizons, the black hole is far from extremality and the inner horizon is very close to $r = 0$. It is quite easy to understand that these quantum effects are completely irrelevant for macroscopic black holes, at least for what concerns the phenomenology accessible to external observers. In fact, the matter density is sensibly different from zero only at distances of order ℓ_P from the classical singularity at $r = 0$. Therefore, for the external observer, the deviations from the Schwarzschild solution are expected to be incredibly small. We have sensible deviations from $r_H \sim R_S$ only for black holes with masses of order the Planck mass $m_P = 1/\sqrt{G}$, where the event horizon is slightly less than R_S (the radius of the outer horizon is $r_H \simeq 1.8\sqrt{G} = 0.9 R_S$). However, as the mass increases, the outer horizon becomes rapidly indistinguishable from R_S. For example, for a solar mass black hole, $M = 1\ M_\odot$, the outer horizon of the metric (72) is at R_S and the corrections are exponentially suppressed by a factor $\Gamma(\frac{3}{2}, \frac{r_H^2}{\ell_P^2}) \sim e^{-r_H^2/\ell_P^2} = e^{-R_S^2/\ell_P^2} = e^{-\frac{4GM_\odot^2}{c\hbar}} \sim e^{-10^{76}}$ (note that, in the last expression, we have reinstated the speed of light c and the Planck constant $\hbar$). The mass deviation at the horizon $\Delta m(r_H)$ is of the same order of magnitude, which is effectively zero from the point of view of the external observer.

2. $\ell \sim R_S$

As explained in the introduction, there are several indications pointing at the relevance of quantum effects at horizon scales. However, presently we do not have a

precise microscopic description of these quantum effects, but only some quite interesting proposals, like, e.g., fuzzballs, firewalls, nonlocal effects and corpuscular models. An interesting explicit corpuscular black-hole model with a Gaussian core is the one given in Ref. [149], whose density profile is

$$\epsilon_{\text{corpuscular}} = \frac{7^2 m_{\text{P}}}{\sqrt{\pi} N} \frac{e^{-\frac{7}{2N}\frac{r^2}{\ell_{\text{P}}^2}}}{\ell_{\text{P}}^3} \tag{82}$$

where N is the number of gravitons building up the black hole. Comparing this profile with our model (67), we can read the values of our parameters ℓ, M in terms of N

$$\ell = \ell_{\text{P}} \sqrt{\frac{2N}{7}}, \qquad M = 49\pi \frac{\ell^3}{N \ell_{\text{P}}^4}. \tag{83}$$

From these equations, one easily gets the expected holographic scaling of N, $N \propto \ell_{\text{P}}^2 M^2$ and a value of ℓ which is $\ell = R_{\text{S}}/28\pi \simeq 0.01 R_{\text{S}} < \ell_c$. The black hole has two horizons and is far from extremality. The outer horizon is quite close to the classical Schwarzschild one, we have $r_{\text{H}} \simeq 0.96 R_{\text{S}}$. Therefore, the mass deviation is again quite small:

$$\left.\frac{\Delta m}{M}\right|_{\text{H}} = \frac{2}{\sqrt{\pi}} \Gamma\left(\frac{3}{2}, y_{\text{H}}^2\right) \sim e^{-7733}. \tag{84}$$

We see that, for a value of ℓ which is about $1/100$ of the critical value ℓ_c, deviations from the classical behavior are still quite small.

As a last example we consider a value $\ell < \ell_c$, but quite close to the critical value, $\ell = \ell_c/2$. The space-time has two horizons and the outer one is at

$$r_{\text{H}} \simeq 0.92 R_{\text{S}}, \tag{85}$$

which is a small, but still important, difference with respect to the classical radius R_{S}. The mass deviation is

$$\left.\frac{\Delta m}{M}\right|_{\text{H}} = \frac{2}{\sqrt{\pi}} \Gamma\left(\frac{3}{2}, \frac{c^4 r_{\text{H}}^2}{G^2 M^2}\right) \simeq \frac{2}{\sqrt{\pi}} \Gamma\left(\frac{3}{2}, 1.84^2\right) \simeq 0.07. \tag{86}$$

These results further show that the most interesting regime is that for which $\ell \sim R_{\text{S}}$ from both a purely theoretical and from a phenomenological points of view.

B. Thermodynamics and phase transition

Inserting the metric function (72) into Eq. (30), we get the temperature and the ADM mass of the Gaussian black holes

$$T_{\text{H}} = \frac{1}{4\pi r_{\text{H}}} \left[1 - \frac{8GM(r_{\text{H}}) r_{\text{H}}^2}{\ell^3} e^{-r_{\text{H}}^2/\ell^2}\right],$$
$$M(r_{\text{H}}) = \frac{r_{\text{H}}}{2G\left[1 - \frac{2}{\sqrt{\pi}} \Gamma\left(\frac{3}{2}, \frac{r_{\text{H}}^2}{\ell^2}\right)\right]}. \tag{87}$$

The temperature is given by the standard Hawking result plus an ℓ-dependent term, encoding quantum deviations from standard black hole thermodynamics, which however are exponentially suppressed. The behavior agrees with the qualitative one depicted in Fig. 2. It starts from zero in correspondence with the extremal case. Then, it rises and reaches a maximum, whose position is given by solving the equation $dT_{\text{H}}/dr_{\text{H}} = 0$, which in the present case is at $r_{\text{H,max}} \simeq 2.38\ell$. Finally, it decreases and reaches zero as $r_{\text{H}}/\ell \to \infty$, in agreement with the fact that we have to recover the standard Schwarzschild results $T_{\text{H}} = \frac{1}{4\pi r_{\text{H}}}$, $M = \frac{r_{\text{H}}}{2G}$ in this limit. Also in this case, the quantum deformation parameter $\ell \neq 0$ solves the singular thermodynamic behavior of the Schwarzschild temperature $T_{\text{H}} \to \infty$ for $r_{\text{H}} \to 0$.

On the other hand, from Eq. (73a), we get the value of the deformation parameter corresponding to $r_{\text{H,max}}$

$$\ell_{\text{H,max}} = \frac{1 - \frac{2}{\sqrt{\pi}} \Gamma\left(\frac{3}{2}, y_{\text{H,max}}^2\right)}{y_{\text{H,max}}} R_{\text{S}} \simeq 0.42 R_{\text{S}}. \tag{88}$$

The entropy of the black hole can be obtained by integrating Eq. (33) numerically, using the fact that the zero-entropy state is at the extremal radius $r_{\text{H,extremal}}/\ell \simeq 1.51$. The result of the integral is presented in Fig. 6 (dashed orange line) and is compared to the standard result for the Schwarzschild black hole.[8] As it can be seen, the entropy does not differ significantly from the standard area law, as quantum deviations are expected to be exponentially suppressed [150–152] [see also Eq. (71)].

Expanding Eq. (87) near extremality yields the quadratic scaling (34) of the mass above extremality with the temperature

$$M - M_c \simeq 15.55 \frac{\ell^3}{G} T_{\text{H}}^2. \tag{89}$$

The specific heat can be computed using Eq. (35) and follows the qualitative behavior of Fig. 3: it diverges at $r_{\text{H,max}} \simeq 2.38\ell$, indicating the onset of the second-order phase transition. Indeed, by computing numerically the free energy $\mathcal{F} = M - T_{\text{H}} S$ and expressing it as a function of T_{H}, we get the phase diagram depicted in Fig. 7.

Again, we have two branches. Branch I corresponds to r_{H} taking values between the extremal value r_c and $r_{\text{H,max}}$

[8] In this case, the blue solid curve in Fig. 6 is obtained by subtracting the Hawking entropy of the extremal configuration $S_{\text{extremal}} = \pi r_{\text{H,extremal}}^2$ (with $G = 1$) from the standard Schwarzschild entropy πr_{H}^2.

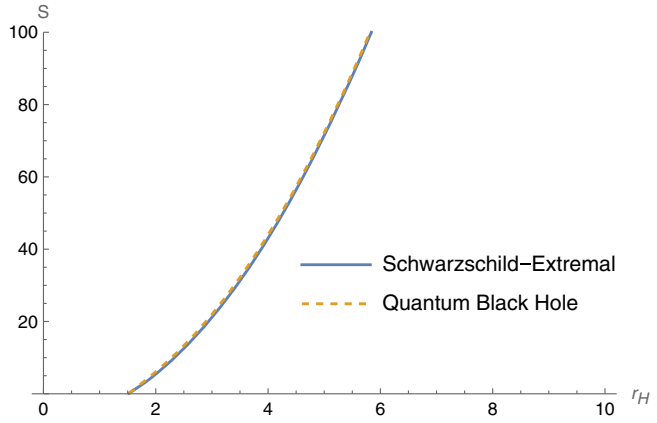

FIG. 6. Plot of the entropy of the quantum Gaussian black hole (dashed orange line) vs standard Hawking entropy of the Schwarzschild black hole (minus the corresponding Hawking entropy of the extremal case). For simplicity, we set $\ell = 1$ and $G = 1$.

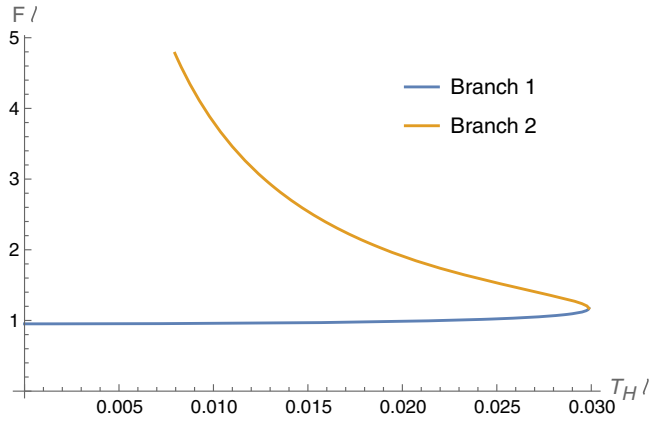

FIG. 7. Free energy $\mathcal{F}$, in units of ℓ^{-1}, as a function of the temperature in units of ℓ^{-1}, for the Gaussian model. We distinguish between two branches: one corresponding to black holes with $\ell \sim R_S$ (solid blue curve), the other (orange curve) corresponding to $\ell \ll R_S$.

(correspondingly, the parameter ℓ takes values between $\ell_{H,max} \simeq 0.42R_S$ and $\ell_c \simeq 0.53R_S$), and therefore describes quantum black holes with $\ell \sim R_S$. Conversely, branch *II* corresponds to r_H much larger than $r_{H,max}$, corresponding to small ($< 0.42R_S$) values for the parameter ℓ. Thus, the far right region of branch *II* describes again classical black holes ($\ell \ll R_S$).

Figure 7 shows that the free energy of branch *I* is always smaller than that of branch *II*. This means that black holes in branch *I*, i.e., black holes with $\ell \sim R_S$, are always energetically preferred.

C. Null geodesics and photon orbits

The effective potential (40) determining photon orbits in the Gaussian quantum black hole reads

$$V(r) = \frac{J^2}{2r^2}\left[1 - \frac{2GM}{r} + \frac{4GM}{\sqrt{\pi} r}\Gamma\left(\frac{3}{2}, \frac{r^2}{\ell^2}\right)\right], \quad (90)$$

and its behavior for different values of the parameter $\alpha \equiv R_S\ell^{-1}$ agrees with the qualitative plots shown in Fig. 4.

The extrema of the potential are given by the zeros of $dV(r)/dr$ [see Eq. (41)], i.e., by the solution of the equation

$$-r + 3GM - \frac{4GM}{\sqrt{\pi}}\frac{r^3}{\ell^3}e^{-r^2/\ell^2} - \frac{6GM}{\sqrt{\pi}}\Gamma\left(\frac{3}{2}, \frac{r^2}{\ell^2}\right) = 0. \quad (91)$$

We see that the presence of ℓ shifts the position of the photon sphere from the Schwarzschild case $r = 3GM$. By numerically solving the equation above, we distinguish again between the three cases (2, 1, or no horizons)

(i) *Two horizons* ($\alpha > \frac{3}{2-\frac{4}{\sqrt{\pi}}\Gamma(\frac{3}{2},\frac{9}{4})}$): we have multiple zeros, corresponding to one minimum in the black-hole interior and one maximum in the exterior, which corresponds to the position of the unstable photon orbit. We are interested in the latter. For instance, for $\alpha = 2$ ($\ell = GM$ therefore), we have $y_m \simeq 2.99$, which corresponds to a position of the photon ring $r_m \simeq 2.99\ell = 2.99GM$, very close to the Schwarzschild case $3GM$.

(ii) *One horizon* ($\alpha = \frac{3}{2-\frac{4}{\sqrt{\pi}}\Gamma(\frac{3}{2},\frac{9}{4})}$): this case is similar to the previous one, we have a minimum (coinciding with the event horizon), which represents a stable photon orbit, and a maximum in the potential, representing the unstable photon orbit. Focusing again on the latter, we have $y_m \simeq 2.84$, corresponding to $r_m \simeq 2.98GM$, again pretty close to the Schwarzschild result.

(iii) *No horizons* ($\alpha < \frac{3}{2-\frac{4}{\sqrt{\pi}}\Gamma(\frac{3}{2},\frac{9}{4})}$): we have two possible cases. If α is large enough ($\alpha \sim [1.6, 1.8]$), we can have a maximum corresponding to a photon ring. For example, for $\alpha = 1.6$, we get $y_m \simeq 2.19$, which means $r_m \simeq 2.74GM$, which is a significant departure from the standard result. However, if α falls below the aforementioned interval, we do not have a maximum anymore and the photon ring cannot be present.

D. Quasinormal modes spectrum in the eikonal limit

We can use the general arguments and results of Sec. IV F to compute the expression of the quasinormal frequencies for the quantum Gaussian black hole in the eikonal limit. Applying the general formulas (48a), (48b) to the case of Eq. (72), we get

$$\omega_{\mathrm{R}} = \frac{l}{\ell y_m}\sqrt{1-\frac{\alpha}{y_m}\left[1-\frac{2}{\sqrt{\pi}}\Gamma\left(\frac{3}{2},y_m^2\right)\right]} \tag{92a}$$

$$\omega_{\mathrm{I}} = -\left(n+\frac{1}{2}\right)\frac{1}{\sqrt{2}\ell}\sqrt{\alpha\left[y_m-\alpha+\frac{2}{\sqrt{\pi}}\Gamma\left(\frac{3}{2},y_m^2\right)\right]\left|\frac{3}{y_m^4}-\frac{4}{\sqrt{\pi}}\frac{1+2y_m^2}{y_m}e^{-y_m^2}-\frac{6}{\sqrt{\pi}y_m^2}\Gamma\left(\frac{3}{2},y_m^2\right)\right|} \tag{92b}$$

By expanding around the critical value α_c (75), we get

$$\omega_{\mathrm{R}} \simeq \frac{l}{\ell}[0.20-0.10(\alpha-\alpha_c)] \simeq 0.20\frac{l}{\ell}-3.36l\ell T_{\mathrm{H}}^2; \tag{93a}$$

$$\omega_{\mathrm{I}} \simeq \frac{1}{\ell}\left(n+\frac{1}{2}\right)[-0.19+0.05(\alpha-\alpha_c)] \simeq -\frac{0.19}{\ell}\left(n+\frac{1}{2}\right)+1.63\left(n+\frac{1}{2}\right)\ell T_{\mathrm{H}}^2. \tag{93b}$$

VII. CONCLUSIONS

In this paper, we explored the possibility of relating long-range quantum gravity corrections at horizon scales with the absence of the central singularity in the Schwarzschild black hole. In order to achieve this, we explicitly constructed a general class of static, nonsingular, asymptotically flat black-hole models as exact solutions of Einstein's field equations sourced by an anisotropic fluid with EoS $p_\parallel = -\varepsilon$. A natural physical consequence of this choice is the fact that these models possess a dS core. This causes a violation of the strong energy condition near the black-hole center, which therefore allows us to circumvent Penrose's singularity theorem.

Analogously to what has been done at galactic and cosmological level [56–61], the anisotropic-fluid source is used to give a multiscale description of the gravitational system and an effective description of the quantum black hole. In our models, quantum corrections are effectively encoded in a *single* additional scale ℓ, which appears as an extra "quantum hair" for the black hole and is related to the dS length $\hat{L}$, smearing the would-be central singularity of the Schwarzschild black hole.

Apart from solving the singularity problem and allowing for quantum effects at horizon scales, our general black-hole solutions have also other rather interesting geometric and thermodynamic features. They allow for the presence of two horizons, an outer event horizon and an inner Cauchy one. When these two merge in a single horizon, we have an extremal configuration, which is a zero-temperature, zero-entropy state, whose near-horizon geometry factors as $\mathrm{AdS}_2 \times \mathrm{S}^2$. This fact could be very useful in addressing the black-hole information puzzle.

The previous features determine a rather nontrivial thermodynamic behavior. The presence of the quantum hair ℓ, not related to a thermodynamic potential, required a generalization of the area law for the black-hole entropy. We also found a metastable behavior and a phase transition, in which black holes closer to extremality, i.e., with $\ell \sim R_{\mathrm{S}}$, are always thermodynamically preferred with respect to those with $\ell \gg R_{\mathrm{S}}$. This means that our "quantum black holes" are thermodynamically preferred with respect to those in which quantum corrections are irrelevant. This provided further evidence for the relevance of quantum effects at horizon scales.

For $\ell \gtrsim R_{\mathrm{S}}$, instead, we found that our models represent horizonless compact object, which however were not investigated in depth in the present paper and will be matter for further investigations.

Finally, we have also shown that, when $\ell \ll R_{\mathrm{S}}$, the phenomenology of our nonsingular black-hole solutions is almost indistinguishable from the standard Schwarzschild-solution one for an outside observer. On the other hand, for $\ell \sim R_{\mathrm{S}}$, there could be manifest signatures of deviations from the standard behavior, both in the photon orbits and in the QNMs spectrum.

For what concerns photon orbits, we have found stable bounded orbits, which are, however, internal to (in the two-horizon model) or coinciding with (in the extremal case) the horizon. An interesting result is that for some horizonless models, unstable photon orbits do not form.

On the QNMs side, we have investigated the spectrum of quasinormal frequencies in the eikonal limit and in the near-extremal limit. We found a scaling behavior with the temperature and a dependence from the quantum hair ℓ. These features have a manifest experimental signature, which could be experimentally accessible in the near future by the next generation of GW detectors. Taking a near-horizon limit together with a near-extremal one, instead, we found an imaginary part which vanishes with the temperature. Our findings only partially confirm Hod's conjecture on zero-damped QNMs for standard extremal black holes [75–81]. On the other hand, this result is perfectly consistent with the $\mathrm{AdS}_2 \times \mathrm{S}^2$ behavior of the near-horizon, near-extremal metric and with what is known about the QNMs spectrum of 2D AdS gravity models [70–74].

We have confirmed our general results by thoroughly investigating two particular cases, which represent two widely known nonsingular black-hole models, namely the Hayward and the Gaussian-core metrics. We have revisited these models considering the quantum deformation parameter of the same order of magnitude of the Schwarzschild radius R_S. This perspective is completely different from the standard approach to these models, where quantum effects, and hence ℓ, are of the order of magnitude of Planck length, implying extremely small and phenomenologically irrelevant deviations from standard behavior.

ACKNOWLEDGMENTS

We thank S. Liberati for useful discussions.

APPENDIX: GEODESIC COMPLETENESS OF THE SPACETIME

In this Appendix, we show that space-times described by Eq. (22) are geodesically complete. We start from Raychaudhuri's equation, which describes the evolution of a timelike geodesic congruence Θ

$$\frac{d\Theta}{d\tau} = -\frac{1}{3}\Theta^2 - \sigma^{\mu\nu}\sigma_{\mu\nu} + \omega^{\mu\nu}\omega_{\mu\nu} - R_{\mu\nu}u^\mu u^\nu, \tag{A1}$$

where τ is the proper time, $u^\mu = dx^\mu/d\tau$ the proper timelike velocity, while $\sigma_{\mu\nu} = \Theta_{\mu\nu} - \frac{1}{3}\Theta h_{\mu\nu}$ is the shear tensor ($h_{\mu\nu} = g_{\mu\nu} + u_\mu u_\nu$ is the transverse metric) and $\omega_{\mu\nu} = h^\alpha_\mu h^\beta_\nu u_{[\alpha;\beta]}$ is the vorticity tensor. If we consider geodesics to be hypersurface orthogonal, then $\omega_{\mu\nu} = 0$. Since both the shear and the vorticity tensors are purely spatial, i.e., $\omega_{\mu\nu}\omega^{\mu\nu} \geq 0$, $\sigma_{\mu\nu}\sigma^{\mu\nu} \geq 0$, and if we assume *the strong energy condition to hold*, i.e., $R_{\mu\nu}u^\mu u^\nu \geq 0$, we expect in all generality a focusing of the geodesic congruence, i.e., $d\Theta/d\tau \leq 0$ and the formation of caustics, which represent singularities of the congruence. This is the essence of the original Penrose singularity theorem [1]. Let us now show that caustics cannot form for the models described by Eq. (22). We consider first a generic metric function A and timelike geodesics

$$g_{\mu\nu}u^\mu u^\nu = -1, \tag{A2}$$

and focus on geodesics on the plane $\theta =$ constant and $\varphi =$ constant. We then have $u^\theta = u^\varphi = 0$. We are left with

$$g_{\mu\nu}u^\mu u^\nu = -1 \Rightarrow -A(r)(u^0)^2 + \frac{(u^r)^2}{A(r)} = -1. \tag{A3}$$

But $u^0 = dt/d\tau = 1/A(r)$ (since the metric redshift factor determines the relation between the coordinate and proper time), and therefore

$$-\frac{1}{A(r)} + \frac{(u^r)^2}{A(r)} = -1 \Rightarrow u^r = \pm\sqrt{1 - A(r)}. \tag{A4}$$

This yields the congruence

$$\Theta = \frac{1}{r^2}\partial_r(r^2u^r) = \frac{1}{r^2}\left[2ru^r + r^2\frac{du^r}{dr}\right] = \pm\left(\frac{2}{r}\sqrt{1-A(r)} - \frac{A'(r)}{2\sqrt{1-A(r)}}\right). \tag{A5}$$

The geodesic congruence evolution as a function of the proper time can therefore be written as

$$\frac{d\Theta}{d\tau} = \frac{d\Theta}{dr}\frac{dr}{d\tau} = \Theta' u^r = -\frac{2(1-A(r))}{r^2} - \frac{A'(r)}{r} - \frac{A''(r)}{2} - \frac{A'(r)^2}{4(1-A(r))}, \tag{A6}$$

where we used the fact that Θ is a function of r only.

Let us now specialize Eq. (A6) to the case given by Eq. (22). We get

$$\frac{d\Theta}{d\tau} = -\frac{2\alpha F(y)}{y^2\ell^2} + \frac{\alpha}{y\ell^2}F'(y) + \frac{\alpha}{2\ell^2}F''(y) - \frac{\alpha}{4\ell^2}\frac{F'(y)^2}{F(y)} \tag{A7}$$

Since, for large y, our general model behaves essentially as the Schwarzschild black hole, we focus on the behavior of the geodesics bundle in the core of the object, i.e., for $y \to 0$, where $F \sim y^2$ according to Eq. (24). Therefore, $F' \sim 2y$ and $F'' \sim 2$, and thus

$$\frac{d\Theta}{d\tau} \sim -\frac{2\alpha}{\ell^2} + \frac{2\alpha}{\ell^2} + \frac{\alpha}{\ell^2} - \frac{\alpha}{\ell^2} \sim 0, \tag{A8}$$

so that we do not encounter a caustic in the center, the bundle of geodesics is defocused and therefore they can be extended beyond $r = 0$. This is consistent with the form of the Penrose diagram for such models (see e.g., Refs. [94,148]), which shows that, apart from the presence of the central singularity, the maximal extension of these space-times is similar to that of RN black holes.

These results can be further confirmed by computing $d\Theta/d\tau$ for the two specific models investigated in detail in the paper, namely the Hayward and the Gaussian-core black holes.

For the Hayward black hole, plugging the function F (51) into Eq. (A7) yields

$$\frac{d\Theta}{d\tau} = -\frac{9\alpha y^3(y^3+4)}{4\ell^2(1+y^3)^3}. \tag{A9}$$

Near $y \sim 0$, we have $\frac{d\Theta}{d\tau} \sim -\frac{9\alpha y^3}{\ell^2} + \mathcal{O}(y^4)$, so no caustic is present in the interior, at $r = 0$.

In the Gaussian-core black-hole case, using the function F (72) into Eq. (A7), we get

$$\frac{d\Theta}{d\tau} = -\frac{\alpha e^{-2y^2}}{4\ell^2\sqrt{\pi}y^3}\cdot\frac{9\pi e^{2y^2}+16y^6+8\sqrt{\pi}e^{y^2}y^3(2y^2-3)-4e^{y^2}(9\sqrt{\pi}e^{y^2}-12y^3+8y^5)\Gamma(\frac{3}{2},y^2)+36e^{2y^2}\Gamma^2(\frac{3}{2},y^2)}{\sqrt{\pi}-2\Gamma(\frac{3}{2},y^2)}. \quad \text{(A10)}$$

Near $y \sim 0$, we have $\frac{d\Theta}{d\tau} \sim -\frac{4\alpha y^2}{\sqrt{\pi}\ell^2} + \mathcal{O}(y^4)$, so that again caustics do not form and the space-time is geodesically complete.

[1] R. Penrose, Gravitational Collapse and Space-Time Singularities, Phys. Rev. Lett. **14**, 57 (1965).
[2] S. W. Hawking and R. Penrose, The singularities of gravitational collapse and cosmology, Proc. R. Soc. A **314**, 529 (1970).
[3] R. Penrose, "Golden Oldie": Gravitational collapse: The role of general relativity, Gen. Relativ. Gravit. **34**, 1141 (2002).
[4] S. W. Hawking, Particle creation by black holes, Commun. Math. Phys. **43**, 199 (1975); **46**, 206(E) (1976).
[5] R. Carballo-Rubio, F. Di Filippo, S. Liberati, and M. Visser, Phenomenological aspects of black holes beyond general relativity, Phys. Rev. D **98**, 124009 (2018).
[6] R. Carballo-Rubio, F. Di Filippo, S. Liberati, and M. Visser, Geodesically complete black holes, Phys. Rev. D **101**, 084047 (2020).
[7] H. Maeda, Quest for realistic non-singular black-hole geometries: Regular-center type, arXiv:2107.04791.
[8] A. Simpson and M. Visser, Regular black holes with asymptotically Minkowski cores, Universe **6**, 8 (2019).
[9] F. S. N. Lobo, M. E. Rodrigues, M. V. d. S. Silva, A. Simpson, and M. Visser, Novel black-bounce spacetimes: wormholes, regularity, energy conditions, and causal structure, Phys. Rev. D **103**, 084052 (2021).
[10] J. Mazza, E. Franzin, and S. Liberati, A novel family of rotating black hole mimickers, J. Cosmol. Astropart. Phys. 04 (2021) 082.
[11] E. Franzin, S. Liberati, J. Mazza, A. Simpson, and M. Visser, Charged black-bounce spacetimes, J. Cosmol. Astropart. Phys. 07 (2021) 036.
[12] E. Ayon-Beato and A. Garcia, Nonsingular charged black hole solution for nonlinear source, Gen. Relativ. Gravit. **31**, 629 (1999).
[13] K. A. Bronnikov, Regular magnetic black holes and monopoles from nonlinear electrodynamics, Phys. Rev. D **63**, 044005 (2001).
[14] I. Dymnikova, Regular electrically charged structures in nonlinear electrodynamics coupled to general relativity, Classical Quantum Gravity **21**, 4417 (2004).
[15] H. Culetu, On a regular charged black hole with a nonlinear electric source, Int. J. Theor. Phys. **54**, 2855 (2015).
[16] I. Banerjee, Signatures of regular black holes from the quasar continuum spectrum, arXiv:2206.06899.
[17] A. Bokulić, T. Jurić, and I. Smolić, Constraints on singularity resolution by nonlinear electrodynamics, arXiv:2206.07064.
[18] A. A. Tseytlin, On singularities of spherically symmetric backgrounds in string theory, Phys. Lett. B **363**, 223 (1995).
[19] A. E. Lawrence and E. J. Martinec, String field theory in curved space-time and the resolution of space—like singularities, Classical Quantum Gravity **13**, 63 (1996).
[20] G. T. Horowitz and A. R. Steif, Spacetime singularities in string theory, Phys. Rev. Lett. **64**, 260 (1990).
[21] L. Modesto, Disappearance of black hole singularity in loop quantum gravity, Phys. Rev. D **70**, 124009 (2004).
[22] P. Nicolini, A. Smailagic, and E. Spallucci, Noncommutative geometry inspired Schwarzschild black hole, Phys. Lett. B **632**, 547 (2006).
[23] L. Modesto, Semiclassical loop quantum black hole, Int. J. Theor. Phys. **49**, 1649 (2010).
[24] P. Nicolini, Noncommutative black holes, the final appeal to quantum gravity: A review, Int. J. Mod. Phys. A **24**, 1229 (2009).
[25] S. Hossenfelder, L. Modesto, and I. Premont-Schwarz, A Model for non-singular black hole collapse and evaporation, Phys. Rev. D **81**, 044036 (2010).
[26] L. Modesto, J. W. Moffat, and P. Nicolini, Black holes in an ultraviolet complete quantum gravity, Phys. Lett. B **695**, 397 (2011).
[27] E. Spallucci and S. Ansoldi, Regular black holes in UV self-complete quantum gravity, Phys. Lett. B **701**, 471 (2011).
[28] M. Sprenger, P. Nicolini, and M. Bleicher, Physics on smallest scales: An introduction to minimal length phenomenology, Eur. J. Phys. **33**, 853 (2012).
[29] C. Bambi, D. Malafarina, and L. Modesto, Non-singular quantum-inspired gravitational collapse, Phys. Rev. D **88**, 044009 (2013).
[30] V. P. Frolov, Information loss problem and a "black hole" model with a closed apparent horizon, J. High Energy Phys. 05 (2014) 049.
[31] R. Casadio, O. Micu, and P. Nicolini, Minimum length effects in black hole physics, Fundam. Theor. Phys. **178**, 293 (2015).
[32] E. Binetti, M. Del Piano, S. Hohenegger, F. Pezzella, and F. Sannino, The effective theory of quantum black holes, arXiv:2203.13515.
[33] A. Almheiri, D. Marolf, J. Polchinski, and J. Sully, Black holes: Complementarity or firewalls?, J. High Energy Phys. 02 (2013) 062.
[34] G. Penington, S. H. Shenker, D. Stanford, and Z. Yang, Replica wormholes and the black hole interior, J. High Energy Phys. 03 (2022) 205.
[35] A. Almheiri, T. Hartman, J. Maldacena, E. Shaghoulian, and A. Tajdini, Replica wormholes and the entropy of Hawking radiation, J. High Energy Phys. 05 (2020) 013.

[36] A. Almheiri, T. Hartman, J. Maldacena, E. Shaghoulian, and A. Tajdini, The entropy of Hawking radiation, Rev. Mod. Phys. **93**, 035002 (2021).
[37] R. Bousso, X. Dong, N. Engelhardt, T. Faulkner, T. Hartman, S. H. Shenker, and D. Stanford, Snowmass white paper: Quantum aspects of black holes and the emergence of spacetime, arXiv:2201.03096.
[38] S. B. Giddings, Nonviolent nonlocality, Phys. Rev. D **88**, 064023 (2013).
[39] S. B. Giddings, A "black hole theorem," and its implications, arXiv:2110.10690.
[40] S. B. Giddings, The deepest problem: Some perspectives on quantum gravity, arXiv:2202.08292.
[41] S. D. Mathur, The Fuzzball proposal for black holes: An elementary review, Fortschr. Phys. **53**, 793 (2005).
[42] S. D. Mathur, The nature of the gravitational vacuum, Int. J. Mod. Phys. D **28**, 1944005 (2019).
[43] S. D. Mathur, The VECRO hypothesis, Int. J. Mod. Phys. D **29**, 2030009 (2020).
[44] E. P. Verlinde, Emergent gravity and the dark universe, SciPost Phys. **2**, 016 (2017).
[45] G. Dvali and C. Gomez, Black hole's quantum N-portrait, Fortschr. Phys. **61**, 742 (2013).
[46] G. Dvali and C. Gomez, Quantum compositeness of gravity: Black holes, AdS and inflation, J. Cosmol. Astropart. Phys. 01 (2014) 023.
[47] G. Dvali, Entropy bound and unitarity of scattering amplitudes, J. High Energy Phys. 03 (2021) 126.
[48] R. Casadio, A. Giugno, O. Micu, and A. Orlandi, Thermal BEC black holes, Entropy **17**, 6893 (2015).
[49] R. Casadio, A. Giugno, and A. Giusti, Matter and gravitons in the gravitational collapse, Phys. Lett. B **763**, 337 (2016).
[50] M. Cadoni, M. Tuveri, and A. P. Sanna, Long-range quantum gravity, Symmetry **12**, 1396 (2020).
[51] G. Dvali and C. Gomez, Self-completeness of Einstein gravity, arXiv:1005.3497.
[52] G. Dvali, G. F. Giudice, C. Gomez, and A. Kehagias, UV-completion by classicalization, J. High Energy Phys. 08 (2011) 108.
[53] G. Dvali, C. Gomez, and A. Kehagias, Classicalization of gravitons and goldstones, J. High Energy Phys. 11 (2011) 070.
[54] M. Maggiore, Physical Interpretation of the Spectrum of Black Hole Quasinormal Modes, Phys. Rev. Lett. **100**, 141301 (2008).
[55] M. Cadoni, M. Oi, and A. P. Sanna, Quasinormal modes and microscopic structure of the Schwarzschild black hole, Phys. Rev. D **104**, L121502 (2021).
[56] M. Cadoni, R. Casadio, A. Giusti, and M. Tuveri, Emergence of a dark force in corpuscular gravity, Phys. Rev. D **97**, 044047 (2018).
[57] M. Cadoni, R. Casadio, A. Giusti, W. Mück, and M. Tuveri, Effective fluid description of the dark universe, Phys. Lett. B **776**, 242 (2018).
[58] M. Tuveri and M. Cadoni, Galactic dynamics and long-range quantum gravity, Phys. Rev. D **100**, 024029 (2019).
[59] M. Cadoni, A. P. Sanna, and M. Tuveri, Anisotropic fluid cosmology: An alternative to dark matter?, Phys. Rev. D **102**, 023514 (2020).
[60] M. Cadoni and A. P. Sanna, Emergence of a cosmological constant in anisotropic fluid cosmology, Int. J. Mod. Phys. A **36**, 2150156 (2021).
[61] M. Cadoni and A. P. Sanna, Unified description of galactic dynamics and the cosmological constant, Classical Quantum Gravity **38**, 135004 (2021).
[62] N. Oshita, Q. Wang, and N. Afshordi, On reflectivity of quantum black hole horizons, J. Cosmol. Astropart. Phys. 04 (2020) 016.
[63] Q. Wang, N. Oshita, and N. Afshordi, Echoes from quantum black holes, Phys. Rev. D **101**, 024031 (2020).
[64] S. Chakraborty, E. Maggio, A. Mazumdar, and P. Pani, Implications of the quantum nature of the black hole horizon on the gravitational-wave ringdown, arXiv:2202.09111 [Phys. Rev. D (to be published)].
[65] S. W. Hawking, Breakdown of predictability in gravitational collapse, Phys. Rev. D **14**, 2460 (1976).
[66] D. N. Page, Information in Black Hole Radiation, Phys. Rev. Lett. **71**, 3743 (1993).
[67] S. D. Mathur, The information paradox: A pedagogical introduction, Classical Quantum Gravity **26**, 224001 (2009).
[68] A. Kitaev and S. J. Suh, The soft mode in the Sachdev-Ye-Kitaev model and its gravity dual, J. High Energy Phys. 05 (2018) 183.
[69] A. Almheiri, R. Mahajan, J. Maldacena, and Y. Zhao, The Page curve of Hawking radiation from semiclassical geometry, J. High Energy Phys. 03 (2020) 149.
[70] A. Lopez-Ortega, Entropy spectra of single horizon black holes in two dimensions, Int. J. Mod. Phys. D **20**, 2525 (2011).
[71] R. Cordero, A. Lopez-Ortega, and I. Vega-Acevedo, Quasinormal frequencies of asymptotically anti-de Sitter black holes in two dimensions, Gen. Relativ. Gravit. **44**, 917 (2012).
[72] J. Kettner, G. Kunstatter, and A. J. M. Medved, Quasinormal modes for single horizon black holes in generic 2D dilaton gravity, Classical Quantum Gravity **21**, 5317 (2004).
[73] S. Bhattacharjee, S. Sarkar, and A. Bhattacharyya, Scalar perturbations of black holes in Jackiw-Teitelboim gravity, Phys. Rev. D **103**, 024008 (2021).
[74] M. Cadoni, M. Oi, and A. P. Sanna, Quasi-normal modes and microscopic description of 2D black holes, J. High Energy Phys. 01 (2022) 087.
[75] S. Hod, Quasinormal resonances of near-extremal Kerr-Newman black holes, Phys. Lett. B **666**, 483 (2008).
[76] S. Hod, Slow relaxation of rapidly rotating black holes, Phys. Rev. D **78**, 084035 (2008).
[77] S. Hod, Quasinormal resonances of a massive scalar field in a near-extremal Kerr black hole spacetime, Phys. Rev. D **84**, 044046 (2011).
[78] S. Hod, Quasinormal resonances of a charged scalar field in a charged Reissner-Nordstroem black-hole spacetime: A WKB analysis, Phys. Lett. B **710**, 349 (2012).
[79] S. Hod, Universality in the relaxation dynamics of the composed black-hole-charged-massive-scalar-field system: The role of quantum Schwinger discharge, Phys. Lett. B **747**, 339 (2015).
[80] A. Zimmerman and Z. Mark, Damped and zero-damped quasinormal modes of charged, nearly extremal black

holes, Phys. Rev. D **93**, 044033 (2016); **93**, 089905(E) (2016).
[81] J. Joykutty, Existence of Zero-damped quasinormal frequencies for nearly extremal black holes, arXiv:2112.05669.
[82] S. Ansoldi, P. Nicolini, A. Smailagic, and E. Spallucci, Noncommutative geometry inspired charged black holes, Phys. Lett. B **645**, 261 (2007).
[83] L. Modesto and P. Nicolini, Charged rotating noncommutative black holes, Phys. Rev. D **82**, 104035 (2010).
[84] C. Lan, Y.-G. Miao, and H. Yang, Quasinormal modes and phase transitions of regular black holes, Nucl. Phys. **B971**, 115539 (2021).
[85] M. Cadoni, Conformal symmetry of gravity and the cosmological constant problem, Phys. Lett. B **642**, 525 (2006).
[86] A. Bonanno and M. Reuter, Renormalization group improved black hole space-times, Phys. Rev. D **62**, 043008 (2000).
[87] M. Niedermaier and M. Reuter, The asymptotic safety scenario in quantum gravity, Living Rev. Relativity **9**, 5 (2006).
[88] A. Bonanno, A. Eichhorn, H. Gies, J. M. Pawlowski, R. Percacci, M. Reuter, F. Saueressig, and G. P. Vacca, Critical reflections on asymptotically safe gravity, Front. Phys. **8**, 269 (2020).
[89] A. Adeifeoba, A. Eichhorn, and A. Platania, Towards conditions for black-hole singularity-resolution in asymptotically safe quantum gravity, Classical Quantum Gravity **35**, 225007 (2018).
[90] J. N. Borissova, A. Held, and N. Afshordi, Scale-invariance at the core of quantum black holes, arXiv:2203.02559.
[91] S. S. Bayin, Anisotropic fluids and cosmology, Astrophys. J. **303**, 101 (1986).
[92] M. Cosenza, L. Herrera, M. Esculpi, and L. Witten, Some models of anisotropic spheres in general relativity, J. Math. Phys. (N.Y.) **22**, 118 (1981).
[93] A. DeBenedictis, D. Horvat, S. Ilijic, S. Kloster, and K. S. Viswanathan, Gravastar solutions with continuous pressures and equation of state, Classical Quantum Gravity **23**, 2303 (2006).
[94] S. A. Hayward, Formation and Evaporation of Nonsingular Black Holes, Phys. Rev. Lett. **96**, 031103 (2006).
[95] C. B. M. H. Chirenti and L. Rezzolla, How to tell a gravastar from a black hole, Classical Quantum Gravity **24**, 4191 (2007).
[96] R. Chan, M. F. A. da Silva, and P. Rocha, Gravastars and black holes of anisotropic dark energy, Gen. Relativ. Gravit. **43**, 2223 (2011).
[97] P. Martin Moruno, N. Montelongo Garcia, F. S. N. Lobo, and M. Visser, Generic thin-shell gravastars, J. Cosmol. Astropart. Phys. 03 (2012) 034.
[98] P. Aluri, S. Panda, M. Sharma, and S. Thakur, Anisotropic universe with anisotropic sources, J. Cosmol. Astropart. Phys. 12 (2013) 003.
[99] H. Culetu, On a regular modified Schwarzschild spacetime, arXiv:1305.5964.
[100] T. Harko and F. S. N. Lobo, Cosmological anisotropy from non-comoving dark matter and dark energy, J. Cosmol. Astropart. Phys. 07 (2013) 036.
[101] G. Raposo, P. Pani, M. Bezares, C. Palenzuela, and V. Cardoso, Anisotropic stars as ultracompact objects in general relativity, Phys. Rev. D **99**, 104072 (2019).
[102] P. Beltracchi and P. Gondolo, Formation of dark energy stars, Phys. Rev. D **99**, 044037 (2019).
[103] J. Kumar and P. Bharti, The classification of interior solutions of anisotropic fluid configurations, arXiv:2112.12518.
[104] I. Musco and T. Papanikolaou, Primordial black hole formation for an anisotropic perfect fluid: initial conditions and estimation of the threshold, arXiv:2110.05982.
[105] S. W. Hawking and G. F. R. Ellis, *The Large Scale Structure of Space-Time*, Cambridge Monographs on Mathematical Physics (Cambridge University Press, Cambridge, England, 2011).
[106] E. Poisson and W. Israel, Inner-Horizon Instability and Mass Inflation in Black Holes, Phys. Rev. Lett. **63**, 1663 (1989).
[107] A. Ori, Inner Structure of a Charged Black Hole: An Exact Mass-Inflation Solution, Phys. Rev. Lett. **67**, 789 (1991).
[108] D. Markovic and E. Poisson, Classical Stability and Quantum Instability of Black Hole Cauchy Horizons, Phys. Rev. Lett. **74**, 1280 (1995).
[109] R. Carballo-Rubio, F. Di Filippo, S. Liberati, C. Pacilio, and M. Visser, On the viability of regular black holes, J. High Energy Phys. 07 (2018) 023.
[110] R. Carballo-Rubio, F. Di Filippo, S. Liberati, C. Pacilio, and M. Visser, Inner horizon instability and the unstable cores of regular black holes, J. High Energy Phys. 05 (2021) 132.
[111] A. Bonanno, A.-P. Khosravi, and F. Saueressig, Regular black holes with stable cores, Phys. Rev. D **103**, 124027 (2021).
[112] A. Giugno, A. Giusti, and A. Helou, Horizon quantum fuzziness for non-singular black holes, Eur. Phys. J. C **78**, 208 (2018).
[113] R. Casadio, A. Giugno, and O. Micu, Horizon quantum mechanics: A hitchhiker's guide to quantum black holes, Int. J. Mod. Phys. D **25**, 1630006 (2016).
[114] R. Casadio, A. Giusti, and J. Ovalle, Quantum Reissner-Nordström geometry: Singularity and Cauchy horizon, Phys. Rev. D **105**, 124026 (2022).
[115] C. Barceló, V. Boyanov, R. Carballo-Rubio, and L. J. Garay, Classical mass inflation vs semiclassical inner horizon inflation, arXiv:2203.13539.
[116] B. Knorr and A. Platania, Sifting quantum black holes through the principle of least action, Phys. Rev. D **106**, 021901 (2022).
[117] S. B. Giddings and A. Strominger, Dynamics of extremal black holes, Phys. Rev. D **46**, 627 (1992).
[118] J. M. Bardeen and G. T. Horowitz, Extreme Kerr throat geometry: A vacuum analog of $AdS_2 \times S^2$, Phys. Rev. D **60**, 104030 (1999).
[119] T. Hartman, K. Murata, T. Nishioka, and A. Strominger, CFT duals for extreme black holes, J. High Energy Phys. 04 (2009) 019.
[120] H. K. Kunduri and J. Lucietti, Classification of near-horizon geometries of extremal black holes, Living Rev. Relativity **16**, 8 (2013).

[121] J. M. Maldacena, J. Michelson, and A. Strominger, Anti-de Sitter fragmentation, J. High Energy Phys. 02 (1999) 011.
[122] A. Almheiri and J. Polchinski, Models of AdS_2 backreaction and holography, J. High Energy Phys. 11 (2015) 014.
[123] A. Almheiri and B. Kang, Conformal symmetry breaking and thermodynamics of near-extremal black holes, J. High Energy Phys. 10 (2016) 052.
[124] R. Jackiw, Lower dimensional gravity, Nucl. Phys. **B252**, 343 (1985).
[125] C. Teitelboim, Gravitation and Hamiltonian structure in two space-time dimensions, Phys. Lett. B **126**, 41 (1983).
[126] D. Grumiller, W. Kummer, and D. V. Vassilevich, Dilaton gravity in two-dimensions, Phys. Rep. **369**, 327 (2002).
[127] S. W. Hawking and D. N. Page, Thermodynamics of black holes in anti-de Sitter space, Commun. Math. Phys. **87**, 577 (1983).
[128] D. Pavon, Phase transition in Reissner-Nordstrom black holes, Phys. Rev. D **43**, 2495 (1991).
[129] E. Witten, Anti-de Sitter space, thermal phase transition, and confinement in gauge theories, Adv. Theor. Math. Phys. **2**, 505 (1998).
[130] A. Chamblin, R. Emparan, C. V. Johnson, and R. C. Myers, Holography, thermodynamics and fluctuations of charged AdS black holes, Phys. Rev. D **60**, 104026 (1999).
[131] X. N. Wu, Multicritical phenomena of Reissner-Nordstrom anti-de Sitter black holes, Phys. Rev. D **62**, 124023 (2000).
[132] M. Cadoni, G. D'Appollonio, and P. Pani, Phase transitions between Reissner-Nordstrom and dilatonic black holes in 4D AdS spacetime, J. High Energy Phys. 03 (2010) 100.
[133] D. Kubiznak and R. B. Mann, P-V criticality of charged AdS black holes, J. High Energy Phys. 07 (2012) 033.
[134] A. Rajagopal, D. Kubizňák, and R. B. Mann, Van der Waals black hole, Phys. Lett. B **737**, 277 (2014).
[135] A. Mandal, S. Samanta, and B. R. Majhi, Phase transition and critical phenomena of black holes: A general approach, Phys. Rev. D **94**, 064069 (2016).
[136] R. Li, K. Zhang, and J. Wang, Thermal dynamic phase transition of Reissner-Nordström anti-de Sitter black holes on free energy landscape, J. High Energy Phys. 10 (2020) 090.
[137] P. Chen, Y. C. Ong, and D.-h. Yeom, Black hole remnants and the information loss paradox, Phys. Rep. **603**, 1 (2015).
[138] R. Banerjee, S. K. Modak, and S. Samanta, Glassy phase transition and stability in black holes, Eur. Phys. J. C **70**, 317 (2010).
[139] W. H. Press, Long wave trains of gravitational waves from a vibrating black hole, Astrophys. J. Lett. **170**, L105 (1971).
[140] V. Ferrari and B. Mashhoon, New approach to the quasinormal modes of a black hole, Phys. Rev. D **30**, 295 (1984).
[141] B. Mashhoon, Stability of charged rotating black holes in the eikonal approximation, Phys. Rev. D **31**, 290 (1985).
[142] V. Cardoso, A. S. Miranda, E. Berti, H. Witek, and V. T. Zanchin, Geodesic stability, Lyapunov exponents and quasinormal modes, Phys. Rev. D **79**, 064016 (2009).
[143] M. S. Churilova, Analytical quasinormal modes of spherically symmetric black holes in the eikonal regime, Eur. Phys. J. C **79**, 629 (2019).
[144] B. F. Schutz and C. M. Will, Black hole normal modes: A semianalytic approach, Astrophys. J. Lett. **291**, L33 (1985).
[145] H. Yang, F. Zhang, A. Zimmerman, D. A. Nichols, E. Berti, and Y. Chen, Branching of quasinormal modes for nearly extremal Kerr black holes, Phys. Rev. D **87**, 041502 (2013).
[146] V. P. Frolov, Notes on nonsingular models of black holes, Phys. Rev. D **94**, 104056 (2016).
[147] M. Molina and J. R. Villanueva, On the thermodynamics of the Hayward black hole, Classical Quantum Gravity **38**, 105002 (2021).
[148] S. Ansoldi, Spherical black holes with regular center: A Review of existing models including a recent realization with Gaussian sources, in *Conference on Black Holes and Naked Singularities*, BH2, Dynamics and Thermodynamics of Blackholes and Naked Singularities (Milano, Italy, 2008).
[149] R. Casadio and A. Orlandi, Quantum harmonic black holes, J. High Energy Phys. 08 (2013) 025.
[150] Y. S. Myung, Y.-W. Kim, and Y.-J. Park, Thermodynamics and evaporation of the noncommutative black hole, J. High Energy Phys. 02 (2007) 012.
[151] R. Banerjee, B. R. Majhi, and S. K. Modak, Noncommutative Schwarzschild black hole and area law, Classical Quantum Gravity **26**, 085010 (2009).
[152] K. Nozari and S. H. Mehdipour, Hawking radiation as quantum tunneling from noncommutative Schwarzschild black hole, Classical Quantum Gravity **25**, 175015 (2008).